Review

Polymer Electrolytes for Lithium-Ion Batteries Studied by NMR Techniques

Vitaly I. Volkov [1,2,*], **Olga V. Yarmolenko** [1], **Alexander V. Chernyak** [1,2], **Nikita A. Slesarenko** [1], **Irina A. Avilova** [1], **Guzaliya R. Baymuratova** [1] and **Alena V. Yudina** [1]

1   Institute of Problems of Chemical Physics RAS, 142432 Chernogolovka, Russia; oyarm@mail.ru (O.V.Y.); sasha_cherniak@mail.ru (A.V.C.); wownik007@mail.ru (N.A.S.); irkaavka@gmail.com (I.A.A.); guzalia.rb@yandex.ru (G.R.B.); gvinok@yandex.ru (A.V.Y.)
2   Scientific Center in Chernogolovka RAS, 142432 Chernogolovka, Russia
*   Correspondence: vitwolf@mail.ru or vitwolf@icp.ac.ru

Abstract: This review is devoted to different types of novel polymer electrolytes for lithium power sources developed during the last decade. In the first part, the compositions and conductivity of various polymer electrolytes are considered. The second part contains NMR applications to the ion transport mechanism. Polymer electrolytes prevail over liquid electrolytes because of their exploitation safety and wider working temperature ranges. The gel electrolytes are mainly attractive. The systems based on polyethylene oxide, poly(vinylidene fluoride-co-hexafluoropropylene), poly(ethylene glycol) diacrylate, etc., modified by nanoparticle (TiO_2, SiO_2, etc.) additives and ionic liquids are considered in detail. NMR techniques such as high-resolution NMR, solid-state NMR, magic angle spinning (MAS) NMR, NMR relaxation, and pulsed-field gradient NMR applications are discussed. ^{1}H, ^{7}Li, and ^{19}F NMR methods applied to polymer electrolytes are considered. Primary attention is given to the revelation of the ion transport mechanism. A nanochannel structure, compositions of ion complexes, and mobilities of cations and anions studied by NMR, quantum-chemical, and ionic conductivity methods are discussed.

Keywords: lithium-ion batteries; nanocomposite polymer electrolytes; ionic conductivity; electrochemical impedance; NMR spectroscopy; pulsed-field gradient NMR

1. Introduction

Today, there is a great demand for highly efficient mobile energy storage devices. They must permanently be improved from economic and environmental points of view and must be safe.

It should be noted that currently existing lithium-ion batteries (LIB) have problems ensuring the safety of their operation and high cost. Attempts to solve these problems have led to the emergence of lithium-ion batteries with a polymer electrolyte, which contains nonvolatile components and does not react with electrode materials [1,2]. In addition, this work is aimed at developing post-lithium systems based on sodium [3,4]. However, they would not solve all LIB problems, especially safety-related ones [5].

The use of polymer electrolytes (PE) in LIB radically solves the safety problem because the use of liquid electrolytes can be associated with self-ignition and even explosion. Solid PEs of the polymer–salt composition in most cases have no acceptable conductivity of 10^{-3} S/cm at room temperature and, therefore, at present, there are especially frequent studies of polymer gel electrolytes, as well as nanocomposites based on them.

Polymer gel electrolytes contain aprotic solvents, which can also be unsafe. As an alternative to volatile solvents, ionic liquids have recently begun to be used and, being molten salts, do not ignite and have no saturated vapor pressure. The presence of ionic liquids (IL) in the electrolyte significantly increases the operating temperature range. Therefore, the use of ILs in the composition of both liquid and polymer electrolytes is very important [6–8].

Another promising class of electrolytes for safe solid-state electrochemical devices is nanocomposite polymer electrolytes (NPEs). Such materials have a wide operating temperature range, provide high ionic conductivity and good physical and mechanical properties, and can serve as separators. Some types of NPE can be obtained by casting from a solution of polymer–lithium salt–nanopowder (SiO_2, TiO_2, etc.) followed by the removal of the inert solvent. The resulting dry membrane is then soaked in a liquid electrolyte. There is another class: nanocomposite network polymer gel electrolytes obtained by the reaction of radical polymerization directly in a liquid electrolyte [9–12].

All electrolytes that operate at ambient temperature can be divided into four main classes:

1. Liquid electrolytes (LE);
2. Solid polymer electrolytes (SPE);
3. Polymer gel electrolytes (PGE);
4. Nanocomposite polymer and gel electrolytes (NPEs).

In this review, primary attention is given to the consideration of ion transport processes in polymer gel electrolytes as the most promising for LIB. The review consists of two parts. First, the composition of electrolyte systems and their conductivity are considered. Second, the mechanisms of ion transport investigated by the nuclear magnetic resonance (NMR) technique are discussed. NMR is a very informative tool for characterizing both the structure and dynamics of processes in polymer gel electrolytes. In this paper, the NMR study of solid polymer electrolytes is not considered in detail since, in 2018, a review on this topic was already published in the same journal [13].

2. Electrolytes for Lithium-Ion Batteries, Compositions and Conductivity

2.1. Liquid Electrolytes

Liquid electrolytes for lithium power sources are still an object of research with the aim of their modification to achieve a more stable and safe operation of the whole electrochemical device, as shown in previous reviews [14–16].

Non-aqueous electrolytes are used in LIBs since lithium is very chemically reactive in aqueous solutions. In addition, aqueous electrolytes have a narrow window of electrochemical stability.

Predominantly, LIBs use a liquid electrolyte based on lithium salts in a mixture of aprotic organic solvents. The electrolyte must have sufficiently high conductivity and be resistant to oxidation and reduction.

The compounds $LiPF_6$, $LiClO_4$, $LiBF_4$, $LiSO_3CF_3$ (LiTf), and $LiN(SO_2CF_3)_2$ are used most frequently as lithium salts. Lithium bis(trifluoromethylsulfonyl)imide is abbreviated as LiTFSI.

The concentration of lithium salt in electrolytes at which the maximum conductivity is reached varies from 0.5 to 1.0 M for different compositions. In [17], an empirical formula was developed to determine the optimal salt concentration of the electrolyte at which the maximum conductivity is achieved. For example, for $LiClO_4$ propylene carbonate solutions, this concentration is 0.5 M, while for the currently most used $LiPF_6$ solutions in mixed carbonate solvents, this concentration is 1.0 mol.

The Handbook of Batteries [18] contains data on the conductivity of various mixed liquid electrolytes. It has also been shown that for electrolytes of composition 1 M $LiPF_6$ in solvent mixtures, the conductivity is higher than electrolytes based on a single solvent.

The upper operating temperature of a liquid organic electrolyte is limited up to 60 °C, at which the redox decomposition of the lithium salt starts, or one of the cosolvents boils. When developing the electrolyte composition, it is necessary to carefully choose the electrolyte salt [19] and the type of solvent [14,20].

The structural formulas of anions of lithium salts used in electrolytes for LIB are shown in Figure 1.

$$PF_6^- \qquad ClO_4^- \qquad BF_4^- \qquad SO_3CF_3^- \qquad N(SO_2CF_3)_2^-$$
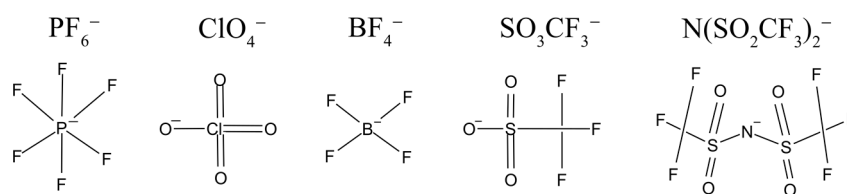
Figure 1. Lithium salt anions are commonly used in electrolytes of LIBs.

The ion mobility increases with decreasing anion size in the series: $LiBF_4$ > $LiClO_4$ > $LiPF_6$ > LiTf > LiTFSI.

These salts are dissolved in aprotic organic solvents with a high dielectric constant (ε), such as ethylene carbonate, EC (ε = 95.3 at 40 °C), propylene carbonate, PC (ε = 65.1), and γ-butyrolactone, GBL (ε = 39). However, because of their high viscosity and low melting temperature (EC melting temperature is about 40 °C), monosolvents are practically not used. In addition to these solvents, so-called thinners with low dielectric constant and low viscosity like dimethyl carbonate (DMC), ethyl methyl carbonate (EMC), diethyl carbonate (DEC), and 1,2-dimethyl ether (DME) are used. Their ε range is from 2.8 to 7.2.

The separator is usually polyethylene (PE) or polypropylene (PP), or a mixture thereof. A multilayer separator is made of layers from different polymers, but a disadvantage of such a separator is poor solvent retention.

Usually, LIBs with organic liquid electrolytes have disadvantages, such as flammability, leakage, and environmental toxicity, making their application difficult [21,22]. In this regard, replacing the liquid electrolyte with a polymer electrolyte seems to be a reliable solution to the aforementioned safety problems.

2.2. Solid Polymer Electrolytes

The first solid polymer electrolyte (SPE) for lithium power sources was proposed by Armand et al. in 1978 [23]. High-molecular-weight polyethylene oxide (PEO), $-(C_2H_4O)_n-$, with a molecular weight of 500 000, was studied as a polymer matrix. The chain with 8 oxygen atoms had 1 Li^+ ion. A hopping mechanism of conduction was assumed. The low conductivity of the SPE composition $(PEO)_8LiClO_4$, about 10^{-8} S/cm at 20 °C, was explained by the high degree of crystallinity of the polymer matrix from a high-molecular-weight linear polymer.

There are quite strict requirements for the selection of the SPE polymer matrix:

- The structure of the main or side chain of the polymer must contain heteroatoms with high basicity, capable of solvating Li^+, thus contributing to the dissociation of the salt;
- Heteroatoms in the polymer chain should be located with such a periodicity that would facilitate the rapid transport of Li^+ ions;
- To ensure the free movement of Li^+ ions, the polymer must not be crystalline, and its glass transition temperature should be lower than the operating temperature of the power source;
- The polymer must be chemically and electrochemically stable with respect to the electrode materials and also be capable of forming mechanically strong films for assembling a chemical power source.

In addition to PEO, the following polymers meet these requirements: polyacrylonitrile (PAN), $-CH_2CH(-CN)-$; polymethyl methacrylate (PMMA), $-CH_2C(-CH_3)(-COOCH_3)-$; polyvinylidene fluoride (PVDF), $-CH_2CF_2-$; etc.

Network polymer electrolytes with a completely amorphous structure are very promising. Such a matrix can be formed by various polyether diacrylates, which, upon radical polymerization, can form a three-dimensional network of different degrees of cross-linking [24]. Among them, poly(ethylene glycol) diacrylate is of interest, where PEO units are located inside. This compound contains units of $-CH_2CH_2O-$ at the edges of the C=C group to form joints.

In some works [25–27], polyethylene glycol methylacrylate (PEG MA) is used. Its formula is $H_2C=CHCO_2(CH_2CH_2O)_nCH_3$. It has a C=C reaction bond on one side only. Therefore, it is used as a copolymer with another oligomer.

The compositions and conductivity of some solid polymer electrolytes are shown in Table 1.

Table 1. The compositions and conductivity of some solid polymer electrolytes.

№	Polymer	Salt	σ, S/cm(T_{room})	Ref.
1	PEO	LiPF$_6$	10^{-5}	[28]
2	Poly(ethylene oxide carbonate)	LiTFSI	7.4×10^{-4}	[29]
3	Allil-PEO/Allil-Gallic acid	LiTFSI	4×10^{-4} at 60 °C	[30]
4	Polypropylene carbonate—PEO	LiTFSI	2×10^{-5}	[31]
5	Crosslinked poly(tetrahydrofuran)	LiTFSI	1.2×10^{-4}	[32]
6	PEG DA	LiClO$_4$	3.5×10^{-6} at 60 °C	[24]
7	PEG MA	LiTFSI	2.13×10^{-4}	[25]
8	Polyglycidyl MA-PEG	LiTFSI	2.1×10^{-5}	[26]
9	PEG-DA-co-PEG MA	LiClO$_4$	10^{-5}	[27]
10	Polystyrene-b-PEO	LiTFSI	2.4×10^{-4}	[33]
11	Cyclodextrin/PEO	LiTFSI	2.44×10^{-6}	[34]

Despite the advantages of SPE, their use is severely limited because the rigid structure of the solid polymer electrolyte demonstrates insufficient ionic conductivity (Table 1).

2.3. Polymer Gel Electrolytes

Polymer gel electrolytes consist of a polymer matrix containing solvents that solvate the ions. Figure 2 shows a schematic representation of the PGE.
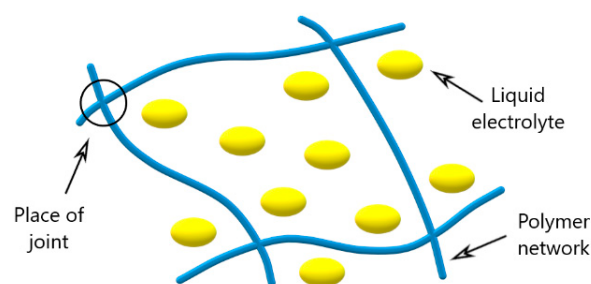
Figure 2. Scheme of cross-linkage of the polymer gel electrolyte.

Gels can be divided into two categories according to their method of preparation:

1. Physical gels are formed when a liquid electrolyte is placed in a polymer matrix without the formation of chemical bonds between the polymer and solvent, for example, a liquid electrolyte solution in PMMA or PVDF;
2. Chemical gels are obtained by chemical cross-linking of a polymer matrix in a liquid organic electrolyte, for example, PEG DA.

The lithium salt is responsible for conduction in the polymer matrix, while the polymer holds the electrolyte to provide mechanical strength. Compared to SPEs, PGEs show higher ionic conductivity, a wide electrochemical stability window, and good compatibility with

electrodes due to their increased ionic mobility. PGEs have both cohesive properties of solids and diffusion properties of liquids, as well as good mechanical strength. In PGE, the role of the polymer is to form a solid matrix that supports the migration of ions in solvents, where a conductivity value of about 10^{-3} S/cm at room temperature can be achieved. Here, the electrolyte can act as a plasticizer, reducing the glass transition temperature, which results in higher ionic conductivity.

If, for SPE, the main matrix is PEO, then the more common polymer matrix for impregnation with liquid electrolyte is poly(vinylidene fluoride-*co*-hexafluoropropylene), $-(CH_2-CF_2)_x-(CF_2-CF(-CF_3))_y-$. The PVDF–HFP copolymer acts as a separation material that swells in an organic liquid electrolyte.

Although high ionic conductivity is an important advantage of PGE over SPE, other characteristics must also be taken into account for the practical use of PGE:

(1)   The ability to retain the liquid phase of the electrolyte;
(2)   Mechanical strength;
(3)   Conductivity in a wide temperature range.

For example, for PGE, solvent losses are often observed due to leakage or evaporation, and, as a result, the cell resistance increases and the contact between the electrodes are broken.

Table 2 lists the composition and characteristics of some polymer gel electrolytes.

Table 2 shows that various polymer gel systems exist. Various polymers, salts, and solvents, including ionic liquids, are used by different researchers.

The safety of gel electrolytes is determined by the degree of fluid retention of the polymer.

The electrochemical stability of the liquid electrolyte at the interface with the electrode is much lower than that of a solid polymer electrolyte. Gel electrolytes have an intermediate composition. Therefore, the stronger the contact between the liquid phase and the electrode, the lower the decomposition potential of the gel electrolyte.

The highest degree of retention of the liquid phase is observed in the mesh matrices formed by chemical crosslinking (PEG-DA, PEDA). PEDA [53,54] is a product of the anionic polymerization of 2-hydroxyethyl acrylate and 4,4'-dicyclohexylmethane diisocyanate. Polar NHCO groups, when introduced into the PEDA chains, favor stronger retention of a polar electrolyte and higher stability of a polymer gel electrolyte.

Table 2. Composition and characteristics of polymer gel electrolytes.

№	Polymer	Electrolyte Composition	σ, S/cm (T_{room})	E, V	Ref.
1	PVDF-HFP	LiBF$_4$ in EC	1.7×10^{-3}	-	[35]
	PVDF-HFP	LiBF$_4$ in GBL	2.5×10^{-3}	5.5	[36]
2	PVDF-HFP		3×10^{-3}		[37]
3	c-PPO [1]	LiPF$_6$ in EC/DMC	0.8×10^{-3}	-	
4	PBO [2]		2×10^{-3}		
5	PVDF-HFP	NaClO$_4$ in EC/DMC/DEC	0.6×10^{-3}	4.6	[38]
6	PVDF-HFP	LiPF$_6$ in isobutyronitrile	17.2×10^{-3}	-	[39]
7		LiTFSI in isobutyronitrile	10.8×10^{-3}		
8		LiPF$_6$ in PC	4×10^{-3}		
9		LiTFSI in PC	5×10^{-3}		
10	PVDF-HFP	LiPF$_6$ in EC/DMC [Pyr$_{14}$] [3] PF$_6$	1.6×10^{-3}	-	[40]
11	PE/PP/PVDF	LiPF$_6$ in EC/DMC/EMC	3×10^{-4}	4.8	[41]
12	PVDF	LiBF$_4$ in PC	10^{-4}	-	[42]
13	PVS [4]/PVDF	LiTFSI in EC/PC	1.74×10^{-3}	4.1	[43]

Table 2. *Cont.*

| №	Polymer	Electrolyte Composition	σ, S/cm (T_{room})	E, V	Ref.
14	PVDF/PEO	LiClO$_4$ in EC/PC	3.03×10^{-3}	5.0	[44]
15	PVDF/methylcellulose/PVDF	LiPF$_6$ in EC/DEM/EMC	1.5×10^{-3}	-	[45]
16	PMMA	LiTFSI/LiBOB [5] in EC/PC	1.33×10^{-3}	-	[46]
17	PMMA	Li[P4441] [6] [TFSI] Li[N4441] [7] [TFSI]	10^{-4}	-	[47]
18	PECA/PET [8]	LiPF$_6$ in EC/DMC	2.54×10^{-3}	4.7	[48]
19	PAN/PEO	LiTf in EC/PC	10^{-3}	-	[49]
20	PEO	LiTFSI in Pyr$_{14}$TFSI	10^{-4}	-	[50]
21	PEO	LiTf in pentyl acetate	10^{-5}	-	[51]
22	MATEMP [9]	NaClO$_4$ in EC/PC	5.13×10^{-3}	5	[52]
23	PEDA	LiClO$_4$ in EC	7.5×10^{-4}	7	[53,54]
24	HBP [10]	LiClO$_4$ in PC	9×10^{-4}	-	[55]
25	PAN elastomer	LiTFSI in PC	3.5×10^{-3}	-	[56]
26	PEG-MA/BEMA [11]	LiTFSI in Pyr$_{13}$TFSI [12]	2.5×10^{-3}		[57]
27	PEG-DA	LiBF$_4$ in EC/PC/BMIBF$_4$ [13]	2.5×10^{-3}	-	[58–89]
30	PEG-DA	LiBF$_4$ in EC/PC/EMIBF$_4$ [14]	4×10^{-3}	-	[60,61]

[1] c-PPO is poly [diemethyl-p-vinyl benzyl phosphonate-co-oligo (ethylene glycol) methacrylate] co-polymer. [2] PBO is poly [benzyl methacrylate-co-oligo (ethylene glycol) ether methacrylate)]. [3] Pyr$_{14}$ is 1-butyl-1-methylpyrrolidinium. [4] PVS is polyvinylstyrene. [5] LiBOB is Lithium bisoxalato borate. [6] [P4441] is tributyl methyl phosphonium. [7] [N4441] is tributyl methyl ammonium. [8] PECA/PET is polyethyl-α-cyanoacrylate/poly (ethylene terephthalate). [9] MATEMP is di(2-methylacryloyltrioxyethyl) methyl phosphonate. [10] HBP is hyperbranched polymer based on methyl methacrylate and triethylene glycol dimethacrylate. [11] BEMA is bisphenol A ethoxylatedimethacrylate. [12] Pyr$_{13}$ is N-Propyl-N-methylpyrrolidinium. [13] BMIBF$_4$ is 1-butyl-3-methylimidazolium tetrafluoroborate. [14] EMIBF$_4$ is 1-ethyl-3-methylimidazolium tetrafluoroborate.

Figure 3 shows the voltammogram of the Li/PE/NS cell for the electrolyte composition PEDA–LiClO$_4$–EC. The upper window of electrochemical stability is almost 7 V vs. Li$^+$/Li [62].

In the membranes based on PVDF-HFP, the retention of the liquid phase is much lower, and, therefore, the solvent has more contact with the electrode material. The electrochemical stability of PVDF-HFP-based electrolytes is 4–5 V. Therefore, works on modifying these membranes are permanently being developed.

Thus, in [45], the authors fabricated a three-layer polymer membrane by placing PVDF on the outer sides. The inner layer was made of methylcellulose, an environmentally friendly and cheap product. The outer layers of PVDF are porous, resulting in a high electrolyte uptake. The resulting Li$^+$ ion transport number was higher than that of the pure methylcellulose-based electrolyte.

Unfortunately, along with a high conductivity of about 10^{-3} S/cm at 20 °C, PGEs have a significant drawback: instability because of a gradual change in the concentration of the organic solvent, which is part of the PGEs, and poor mechanical strength. One of the solutions to these problems is the introduction of nanodispersed additives into the PGE composition and the transition to the so-called class of nanocomposite polymer electrolytes (NPEs).
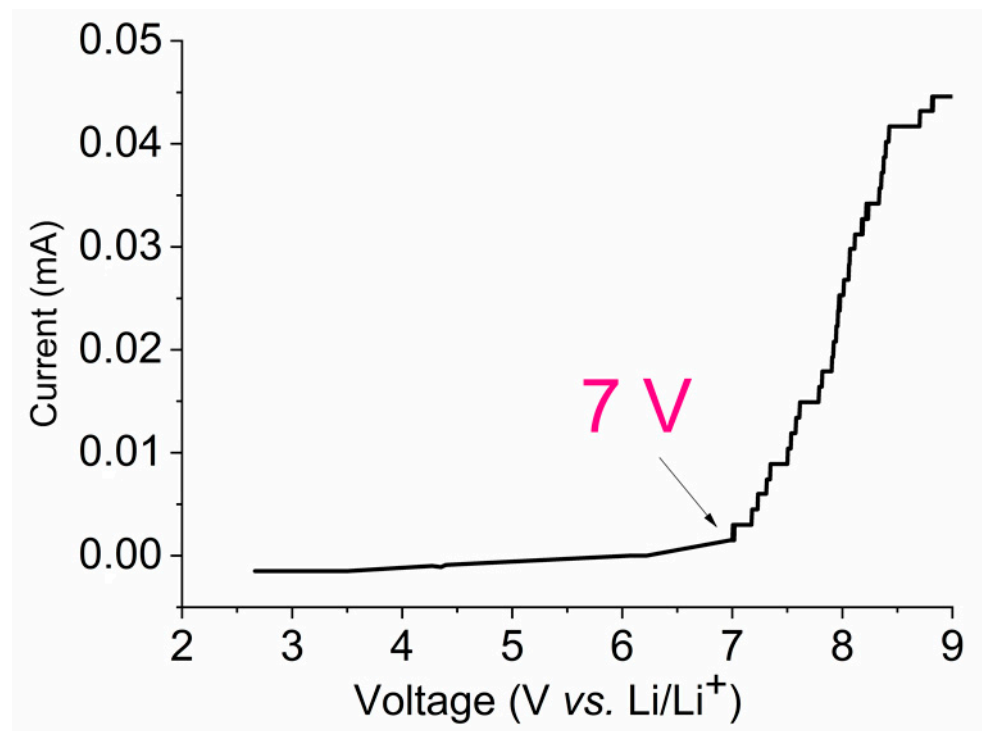
Figure 3. Voltammogram of Li/PGE/Stainless Steel at 2 mV/s rate scanning with PEDA:EC (1:1 *w/w*) and LiClO$_4$ 7.5 wt %.

2.4. Nanocomposite Polymer Electrolytes

Nanocomposite polymer electrolytes for lithium power sources are a promising class of electrolytes for fully solid lithium and lithium-ion batteries, which have increased operational safety [10,11].

Initially, nanoadditives of oxides Al$_2$O$_3$, SiO$_2$, TiO$_2$, etc. were introduced into the SPE matrix to reduce the crystallinity of the polymer and remove traces of moisture because these substances are desiccants.

However, this approach could not radically solve the problem of low conductivity. Nanoparticles then began to be introduced into the composition of PGEs [63]. These works appeared more than 15 years ago. Thus, a new class emerged: nanocomposite polymer gel electrolytes, which are a compromise option that combines the liquid phase conductivity of PGEs and the improved mechanical properties of solid NPEs.

In addition to increasing conductivity and mechanical strength, nanoparticles can reduce the resistance at the electrode/electrolyte interface by shortening the contact area of the liquid phase with the electrode surface. Consequently, the window of electrochemical stability of the electrolyte can expand.

The same polymers, salts, and solvents can be used as the NPE matrix for both SPEs and PGEs, where these solvents act as polymer plasticizers.

For example, Table 3 shows the compositions and conductivity of some recently developed NPEs. Electrolytes nos. 1–7 are solid NPEs. Their composition is a polymer–salt nanoparticle with a conductivity of 10^{-4}–10^{-6} S/cm. The other NPE compositions have an additional liquid phase.

Table 3 shows that the majority of the gel NPEs have a conductivity of about 10^{-3} S/cm at T_{room}, and the best particles for filling are TiO$_2$ and SiO$_2$. These nanoparticles improve the mechanical strength of the gels and contribute to the conductivity of lithium and sodium ions. As shown in [64,65], SiO$_2$ nanoparticles are involved in the dissociation of the electrolyte salt and, hence, the number of charge carriers increases.

In addition to NPEs, there are also hybrid polymer electrolytes [9,66,67], where the role of nanoparticles is played by other particles, for example, octavinyloctasilsesquioxane (POSS) [68,69] or lithium polyvinyl alcohol oxalate borate [70].

Table 3. Compositions and properties of the nanocomposite polymer electrolytes.

№	Polymer	Electrolyte Composition	Nanoparticle	Conductivity, S/cm at T_{298K}	Ref.
1	PEO	LiClO$_4$	SiO$_2$	1.1×10^{-4}	[71]
2	PEO	LiI	LiAlO$_2$	0.6×10^{-3}	[72]
3	PEO	LiTFSI	Gd$_{0.1}$Ce$_{0.9}$O$_{1.95}$	1.9×10^{-4}	[73]
4	PEO	LiTFSI	perovskite La$_{0.8}$Sr$_{0.2}$Ga$_{0.8}$Mg$_{0.2}$O$_{2.55}$	1.3×10^{-4}	[73]
5	PEG-DA	LiTFSI	ZrCl$_4$	8×10^{-6}	[74]
6	PEG MA—PEG DA	LiClO$_4$	SiO$_2$	3.8×10^{-5}	[75]
7	PVDF-HFP	LiTFSI	Li$_{0.33}$La$_{0.557}$TiO$_3$/Li$_3$PO$_4$	5.1×10^{-4}	[76]
8	PEO	LiTFSI, succinonitrile	Li$_{0.33}$La$_{0.557}$TiO$_3$	10^{-3}	[77]
9	PEO	LiClO$_4$ in EC	SiO$_2$	0.2×10^{-3}	[78]
10	PEO/PEG	LiCF$_3$SO$_3$, dioxyphthalate	Al$_2$O$_3$	7.6×10^{-4}	[79]
11	PEG$_{500}$	LiCF$_3$SO$_3$, DME	LiNO$_3$, TiO$_2$	1×10^{-3}	[80]
12	PVA [1]/chitosan	LiClO$_4$	TiO$_2$	2.5×10^{-3}	[81]
13	PVDF-HFP	LiPF$_6$ in EC/DEC	SiO$_2$	0.6×10^{-3}	[82]
14	PVDF-HFP	LiBF$_4$ in GBL	SiO$_2$	3.7×10^{-3}	[36]
15	PVDF-HFP	LiTFSI in EC/DMC	ZnS	3.3×10^{-3}	[83]
16	PVDF-HFP	NaPF$_6$ in EC/PC	TiO$_2$	1.3×10^{-3}	[84]
17	PVDF-HFP	NaTf in EC/PC	SiO$_2$	4×10^{-3}	[85]
18	PVDF-HFP	NaCF$_3$SO$_3$/BMICF$_3$SO$_3$ [3]	TiO$_2$	0.4×10^{-3}	[86]
19	PVC/PEMA [2]	LiClO$_4$ in PC	TiO$_2$	7.1×10^{-3}	[87]
20	PPO-PEO-PPO [4]	LiTFSI in EC/DMC	SiO$_2$	1.32×10^{-3}	[88]
21	P(MMA-*co*-BA)/PE [5]	1M LiPF$_6$ in EC/DMC	SiO$_2$	2.26×10^{-3}	[89]
22	PMMA	LiClO4 in PC	TiO$_2$	3×10^{-4}	[90]
23	PEDA	LiClO$_4$ in EC	TiO$_2$	1.8×10^{-3}	[91,92]
24	PEDA	LiClO$_4$ in EC	Li$_2$TiO$_3$	7×10^{-4}	[92,93]
25	Polyester-polycarbonate	LiTFSI	ZrO$_2$	$\sim 10^{-3}$	[93]
26	PEG-DA	LiBF$_4$ in GBL	SiO$_2$	4.3×10^{-3}	[94]

[1] PVA is polyvinyl alcohol. [2] PVC/PEMA is poly (vinyl chloride)/poly(ethyl methacrylate). [3] BMICF$_3$SO$_3$ is 1-butyl-3-methylimidazolium trifluoromethanesulfonate. [4] PPO is poly(propylene oxide). [5] P(MMA-*co*-BA)/PE is poly(methyl methacrylate-*co*-butylacrylate).

3. NMR Study of Polymer Electrolytes

The synthesis of new polymer electrolytes with desired properties and their efficient use requires establishing a relationship between the structure of the polymer matrix, the features of ion solvation, the structure of transport channels, and the parameters of electro mass transfer, in particular, ionic conductivity and translational ionic and molecular mobility. The impedance spectroscopy method allows one to measure the integral ionic conductivity but provides no information about charge carriers. An important advantage of NMR techniques, especially pulsed field gradient NMR, is the ability to selectively measure the mobilities and self-diffusion coefficients for all ions and molecules involved in charge transfer, for example, solvents (^{1}H and ^{13}C NMR), lithium cations (^{7}Li NMR), and anions (^{11}B, ^{19}F NMR).

In this review, we consider works studying polymer electrolytes of all three classes by NMR methods.

This review summarizes the results of studies carried out by NMR spectroscopy, NMR relaxation, and pulsed magnetic field gradient NMR. Such an analysis makes it possible to establish a number of fundamental regularities of ionic and molecular transport in polymer electrolytes at the molecular level.

NMR is widely applied for polymer electrolytes. The main direction of investigations is lithium cation surroundings, local and macroscopic mobilities of Li^{+} and F^{−}-containing fragments, and electrolyte composition–ion transport correlations. Modern and complicated NMR techniques are employed, especially solid-state high resolution magic angle spinning (MAS) NMR, pulsed-field gradient NMR, and NMR spin relaxation [13,29,32–34,37,39,40,42,47, 49–54,56–61,65,72,73,76,77,80,92,95–128].

3.1. NMR in Solid Polymer Electrolytes

In this paper, the NMR study of solid polymer electrolytes is not considered in detail since, in 2018, a review on this topic was already published in the same journal [13].

In this chapter, NMR studies of SPE are briefly reviewed.

Solid polymer electrolytes of a polymer–salt composition are studied by different NMR methods. The review [108] is devoted to solid-state NMR spectroscopy for the characterization of the molecular structure and dynamics in solid polymers and hybrid electrolytes. In the authors' opinion, the NMR techniques may be very valuable for materials of lithium- and sodium-based batteries. There are solid-state NMR, pulse field gradient NMR, electrophoretic NMR, variable temperature T_1 relaxation, T_2 relaxation and line width analysis, exchange spectroscopy, cross-polarization, rotational echo double resonance, and isotope enrichment applications.

Let us enumerate the most interesting NMR results in other works.

^{7}Li and ^{19}F NMR provide information related to local ion dynamics and diffusion coefficients in poly(ethylene oxide) polymer electrolytes that correlate with the conductivity behavior [116].

Two different Li^{+} positions in the PEO/Li^{+} complex structures were observed by solid-state NMR. The 2D ^{7}Li exchange NMR showed the exchange process between the different Li^{+} species. The exchange dynamics of the Li^{+} ions provide the molecular mechanism of the Li^{+} transportation on the surface of PEO crystal lamella, which correlates with the ionic conduction mechanism [51].

MAS NMR [7]Li in poly(ethylene oxide carbonate) with methacrylic monomer showed that the Li^{+} coordination surrounding depends on the LiTFSI concentration [29].

MAS NMR, PFG NMR, NMR relaxation, and two-dimensional exchange 2D EXSY NMR were applied to LISICON-, NASICON-, and Garnet-type lithium-ion conductors. Two ion diffusion pathways for Li^{+} cation were observed [103].

Comb-like solid polymer electrolytes were studied using cross-polarization ^{13}C-^{1}H solid-state NMR. A correlation between ^{13}C solid-state NMR measurements and phase segregation was determined. ^{7}Li NMR spectroscopy was used to characterize the mobility of lithium ions. It was suggested that lithium ions interact with the PEG-MA pendant groups [107].

^{1}H, ^{7}Li, and ^{19}F NMR were applied to selectively investigate polymer, cation, and anion dynamics in mixing non-entangled poly(propylene glycol) (PPG) with LiClO$_4$ or LiTFSI polymer electrolytes of various length and time scales and over broad temperature ranges. It was observed by static field gradient diffusometry that the long-range motion of all components slows down with increasing salt concentration. Cations are less mobile compared to anions. The Arrhenius temperature dependence does not approximate the ionic diffusion coefficients. It was shown by spin-lattice and spin-spin relaxation that the local lithium and polymer dynamics depend on the salt content. The segmental motion is bimodal for intermediate salt concentrations because two regions (salt-rich and salt-depleted) coexist. Lithium-ion transport is strongly related to polymer segmental motion. The reorganization of polymer chains and lithium-ion transport is controlled by the Rouse dynamics [112].

Fast lithium-ion transport in the crystalline polymer electrolytes was found. The polymer electrolyte composition CD-PEOn/Li$^+$ (*n* = 12, 40) was prepared by self-assembly of α-cyclodextrin (CD), polyethylene oxide, and Li+ salts. The solid-state NMR method combined with the X-ray diffraction technique reveals the following structural features: (a) ordered long-range pathways are formed by CD associates for Li+ ion transport; (b) a sequence of the PEO chains in the tunnels appeared, attenuating the coordination of Li+ significantly by the EO segments [114]. As revealed from ^{1}H and ^{7}Li NMR, the polymer electrolyte based on low-molecular-weight PEOs and cyclodextrin exhibits extremely fast Li+ ion transport [34].

3.2. NMR of Liquid Electrolytes

Some recent NMR data in liquid electrolytes are found in [42,95,98,100,102,120,121].

NMR techniques are used to study ion transport in liquid electrolytes and assess the composition of the solvate environment of ions. Therefore, in [95], the dissociation of LiPF$_6$ in the nonaqueous cyclic propylene carbonate was revealed by ^{7}Li NMR Overhauser enhancement spectroscopy. The coordination number of the solvent and average sizes of solvated and ion-paired clusters were estimated from the PFG NMR data.

Self-diffusion of ^{1}H, ^{7}Li, and ^{19}F was studied in the electrolytes containing LiTFSI salt dissolved in *tert*-butyl methyl ether (MTBE) or tetrahydrofuran (THF) and propylene carbonate (PC), depending on the concentration. At the concentration 1:16 LiTFSI:MTBE and 1:16 LiTFSI:THF, the self-diffusion coefficients decrease with increasing temperature due to ion aggregation. Ionic conductivities increase with increasing temperature [129].

In addition, to characterize the liquid electrolyte itself, its mobility in the pores of separators (PVDF [42] or PE [98]) or electrodes [100] may also be studied by NMR. Self-diffusion coefficients of lithium cations, BF$_4$ anions, and solvent molecules were measured by PFG ^{7}Li, ^{19}F and ^{1}H NMR in LiBF$_4$, propylene carbonate, and PVDF, respectively [42]. Restricted diffusion of a LiPF$_6$ electrolyte solution in porous polyethylene was observed by PFG ^{1}H, ^{19}F, and ^{7}Li NMR, and some structural parameters were estimated [98]. MAS and PFG NMR were used to measure the self-diffusion coefficients of LiPF$_6$ in EC/DMC for electrode pore characterization [100].

The study of liquid electrolytes by high-resolution NMR spectroscopy is considered in more detail.

Solutions of LiBF$_4$ and LiClO$_4$ in ethylene carbonate (EC) were studied by high-resolution ^{1}H, ^{7}Li, ^{11}B, ^{13}C, ^{17}O, ^{35}Cl NMR spectroscopy as model systems [120,121].

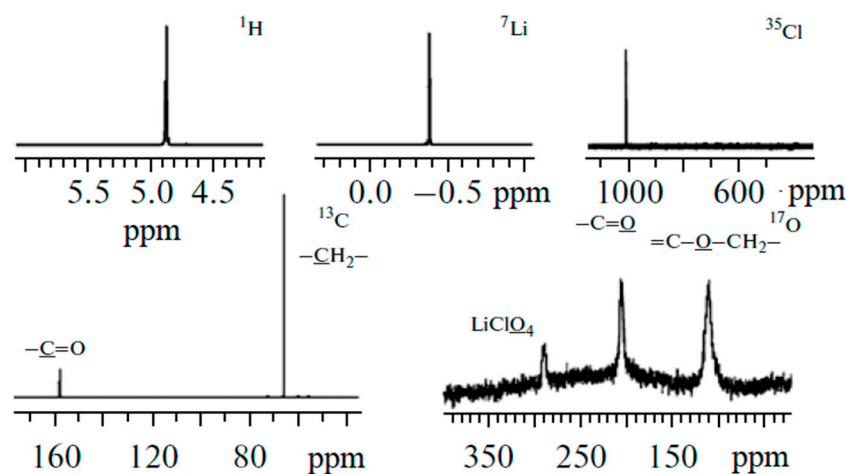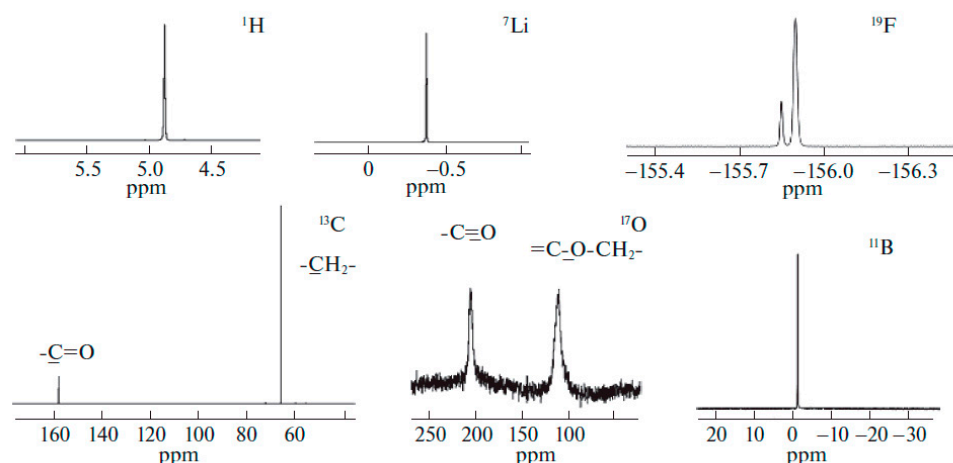The corresponding NMR spectra are shown in Figures 4 and 5.

Figure 4. ^{1}H, ^{7}Li, ^{35}Cl, ^{13}C, and ^{17}O NMR spectra of LiClO$_4$–ethylene carbonate solutions [120].

Figure 5. Experimental ^{1}H, ^{7}Li, ^{19}F, ^{13}C, ^{17}O, and ^{11}B NMR spectra of a 0.66 molality solution of LiBF$_4$ in ethylene carbonate [121].

The quantum-chemical calculations of nuclear chemical shifts were performed. The structure models of cation-anion-solvent complexes depending on concentration were proposed on the basis of a comparison of the experimental and calculated chemical shifts. Some examples of the complex structure are shown in Figures 6 and 7.
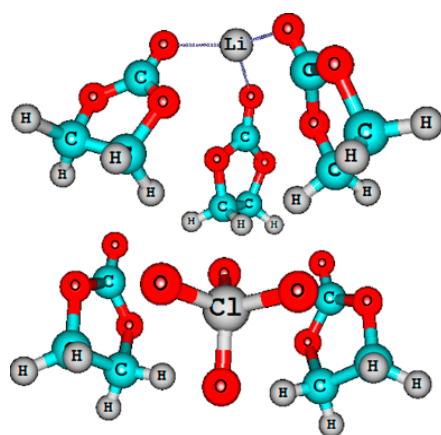
Figure 6. Molecular structures of ionic pair in a 3 molarity LiClO$_4$–ethylene carbonate solution [120].

(**a**)   (**b**)
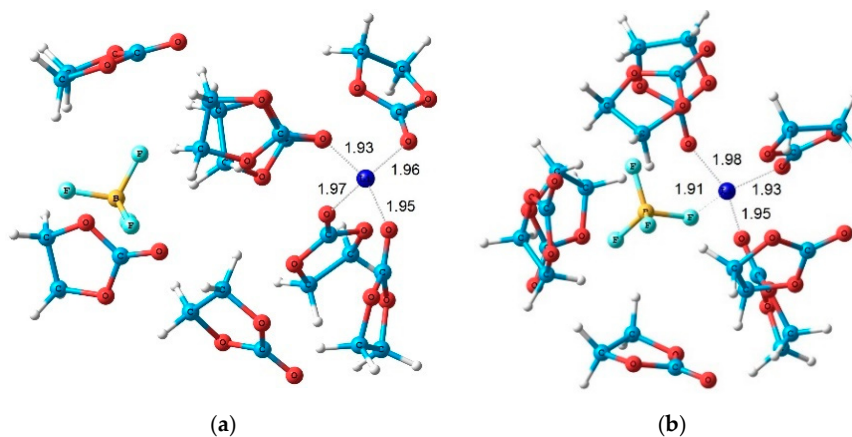
Figure 7. Theoretical structures of (**a**) Li$^+$–4ECs and BF$_4$ –4ECs solvate-separated ion pair and (**b**) LiBF$_4$–8ECs contact ion pair. EC: ethylene carbonate. Interatomic distances are given in angstrom [121].

An analysis of the nuclear chemical shift dependences on the concentration made it possible to calculate the degree of dissociation for $LiBF_4$ in EC [121]. At a low concentration, Li^+ ions are surrounded by the solvate shell only and isolated. Ion solvate-separated and contact ion pairs are formed when the concentration increases [121].

3.3. NMR in Polymer Gel Electrolytes

The results of the NMR study of gel electrolytes are given in [39,40,47,49,50,53,54,56, 57,80,119,122,124–126,130].

Gel-polymer electrolytes are studied mainly by PFG NMR and MAS NMR. In [80], the lithium transport number, ionic association degree, and self-diffusion coefficients were measured in a polyethylene glycol dimethyl ether (MW 500) dissolved in a $LiCF_3SO_3$ electrolyte.

In addition to the experimental methods of NMR and AC impedance spectroscopy, the method of molecular dynamics (MD) is also used. MD is mainly applied to solid polymer [131] or liquid [132] electrolytes. The gel polymer electrolytes are considered in only one paper [32].

Molecular dynamics and density functional theory simulations and ^7Li NMR in crosslinked poly(tetrahydrofuran) (xPTHF) show a decrease in the content of oxygen atoms in the xPTHF backbone, which leads to loosening of O^-Li^+ coordination that enhances ion transport [32]. Gel polymer electrolytes based on PVDF-HFP-containing propylene carbonate, isobutyronitrile (IBN), and trimethyl acetonitrile (TMAN) solvent blend electrolytes were developed. Electrochemical impedance spectroscopy, PFG NMR, and relative permittivity determination revealed remarkable ion-conducting properties of IBN and TMAN solvents [39]. Spin-lattice relaxation times (T_1) and self-diffusion coefficients of ^7Li and ^{19}F were measured in the gel polymer electrolytes based on a polyacrylonitrile elastomer. This study shows that a high acrylonitrile content in the polymer and a solvent with a moderate donor number increase the Li^+ mobility [56].

A very important question is Li^+ cation surroundings. Unfortunately, the ^7Li chemical shift is varied within a range of only 1–2 ppm, which is comparable with the NMR line width even in the MAS spectra. Some results of ^7Li NMR spectra deconvolution are discussed below.

Gel polymer electrolytes based on polyester diacrylate PEDA and ethylene carbonate were investigated. The polymer electrolyte compositions are shown in Table 4 [53].

Table 4. Compositions of the polymer electrolytes.

PGE Composition No.	PGE Starting Components, wt %			
	PEDA	**EC**	**LiClO₄**	**Benzoyl Peroxide**
1	90.5	-	8.1	1.4
2	86.6	4.3	7.8	1.3
3	82.9	8.3	7.5	1.3
4	79.7	12.0	7.1	1.2
5	73.8	18.4	6.7	1.1
6	68.7	24.0	6.3	1.0
7	54.6	36.4	7.6	1.4
8	45.6	45.5	7.5	1.4
9	36.5	54.8	7.3	1.4

The ^7Li NMR spectra are asymmetric and can be decomposed into two singlet lines that differ in width and chemical shift (Figure 8). The ^7Li NMR spectrum of the polymer without solvent is a wide singlet line. In the polymer-solvent system, two NMR lines are observed, the chemical shifts and width of which depend on the EC content. It was

concluded that the narrow line was due to mobile Li^+ coordinated by EC molecules, and the wide line belonged to Li^+ that interacted with the polymer matrix.
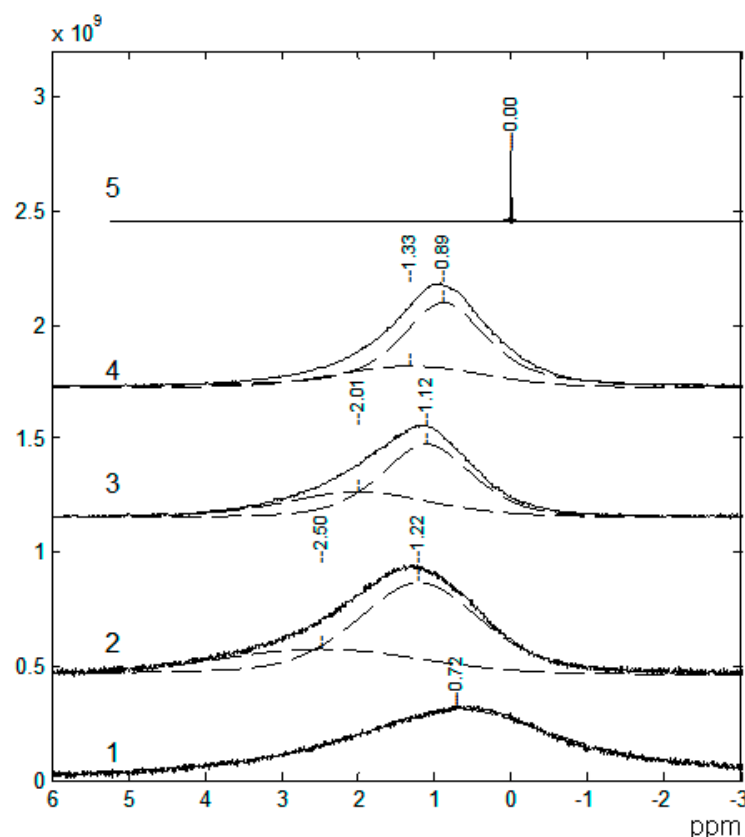
**Figure 8.** ^7Li NMR spectra: 1, sample no. 1; 2, sample no. 2; 3, sample no. 5; 4, sample no. 9; 5, 1 M $LiClO_4$ solution in ethylene carbonate [53].

Gel electrolytes with the addition of tetraethoxysilane were studied [123]. The MAS ^7Li spectra were recorded in the temperature range of $-140\ ^\circ C$ to $80\ ^\circ C$. At low temperatures, Li^+ forms a complex with the polymer. At high temperatures, Li^+ is coordinated by solvent molecules.

The ^7Li NMR spectra of the composite electrolyte gel, PVDF-HFP, with the addition of silicate aerogel (SAG) and ethylene carbonate and propylene carbonate as solvents at different contents of aerogel and $LiClO_4$ are shown in Figure 9 [122].

Four spectrum components were revealed: the peak at 0.104 ppm in gel electrolyte without SAG shows ion pairs and aggregates, the peak at 0.07 ppm belongs to Li^+ interacting with PVDF-HFP fluorine atoms, and the peaks at 0.13 and 0.21 ppm are Li^+ coordinated by PC and EC, respectively [124,125]. The shape and intensity of individual component lines are changed with SAG addition (12 wt %). This indicates the interaction of SAG and Li^+ in the solvent phase and a decrease in the ion pair fraction, which is consistent with the conductivity data. Therefore, it may be concluded that Li^+ cations interact with SAG, solvent, and PVDF-HPF. These interactions could be favored by the formation of transport conditions for the fast movement of Li^+ cations over the SAG particles' surface.
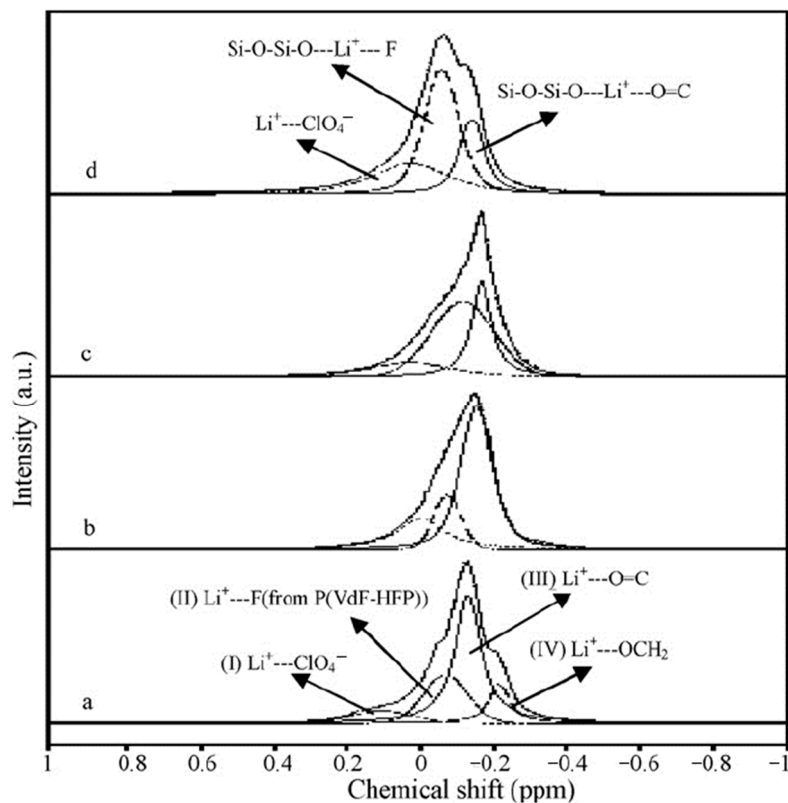
Figure 9. MAS ^{7}Li spectra of (PVDF-HFP)-(PC + EC)-LiClO$_4$-SAG. Component contents (wt %): 20:70:10:0 (**a**), 20:69:10:1 (**b**), 20:66:10:4 (**c**), 20:64:10:6 (**d**). Spinning frequency is 2 kHz [122].

The ^{7}Li diffusion decay is approximated by Equation (1) [126], Figure 10.

$$A(g) = A(0) \exp\left(-\gamma^2 g^2 \delta^2 t_d D_s\right),$$
(1)

where A is the echo signal intensity at the magnetic field gradient pulse with the amplitude g, A_0 is the echo signal intensity without gradient pulse, δ is the duration of the magnetic field gradient pulse, Δ is the interval between the gradient pulses, γ is the nuclear gyromagnetic ratio, and D_s is the self-diffusion coefficient.
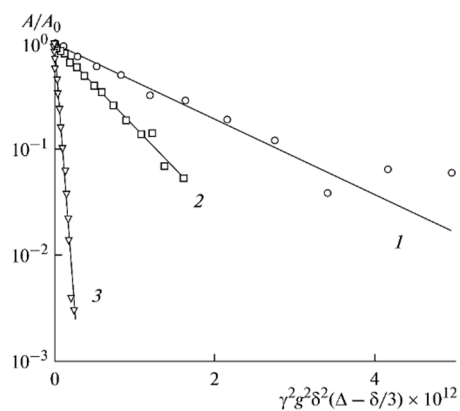
Figure 10. Dependences of the ^{7}Li spin-echo signal amplitudes on the square of magnetic field gradient amplitude (diffusion decay) for PGE samples: (**1**) no. 2, (**2**) no. 5, and (**3**) no. 9 [53].

As shown in Figure 10, the translational motion of Li$^+$ cations is characterized by the self-diffusion coefficient only regardless of the EC content. The diffusion decay shape of ^{1}H is more complicated (Figure 11) and can be decomposed into three exponential

components described by Equation (2) [126]. The self-diffusion coefficient of H atoms can also be characterized by the average coefficient.

$$A(g) = p_1 \exp\left(-\gamma^2 g^2 \delta^2 t_d D_{s1}\right) + p_2 \exp\left(-\gamma^2 g^2 \delta^2 t_d D_{s2}\right) + p_3 \exp\left(-\gamma^2 g^2 \delta^2 t_d D_{s3}\right) \quad (2)$$
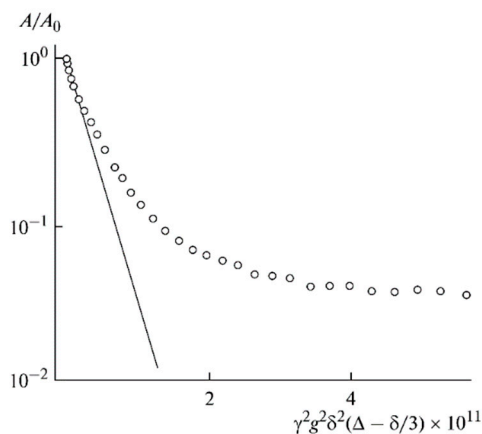
Figure 11. Example of ^{1}H diffusion decay in PGE sample no. 7 [53].

The ionic conductivities σ_{NMR} were calculated from Li$^+$ self-diffusion coefficients using the Nernst–Einstein Equation (3).

$$\sigma = Ne^2 \frac{D}{kT} \quad (3)$$

where N is the number of Li$^+$ ions per unit volume, e is the electron elemental charge, k is the Boltzmann constant, T is the absolute temperature, and $D_{\text{Li+}}$ is the Li$^+$ self-diffusion coefficient.

Figure 12 shows the calculated conductivity σ_{NMR} and experimental conductivity σ_{exp} measured by the impedance spectroscopy dependences on ethylene carbonate content.
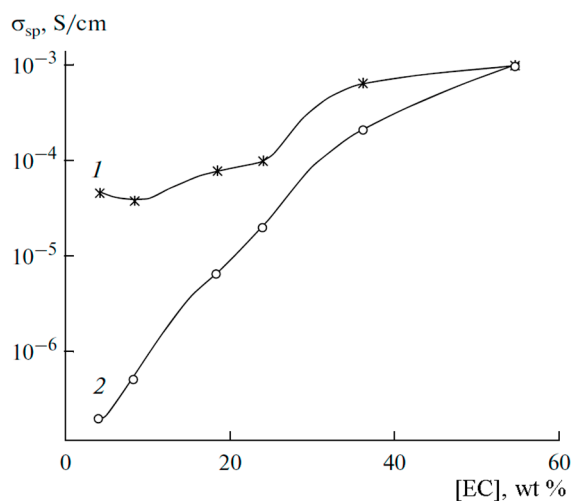
Figure 12. Dependences of the conductivity on the solvent content in PGE at 30 °C: (**1**) conductivity calculated by Equation (3), and (**2**) conductivity measured by impedancemetry [53].

Conductivities increase with a decrease in the polymer concentration. At low EC contents, the calculated conductivity exceeds the measured values by 1–2 orders of magnitude, but the calculated and measured values are equal at the maximum EC.

This fact is explained by the fact that in Equation (3), N is the number of Li$^+$ cations supposing that all perchlorate molecules are dissociated, which occurs at a high EC content only (experimental and calculated conductivities are equal), whereas at low EC LiClO$_4$

molecules are incompletely dissociated. The degree of dissociation α can be calculated as the ratio $\alpha = \sigma_{sp}/\sigma_{NMR}$.

The temperature dependences of the ionic conductivity and lithium self-diffusion coefficient are shown in Figures 13 and 14, respectively.
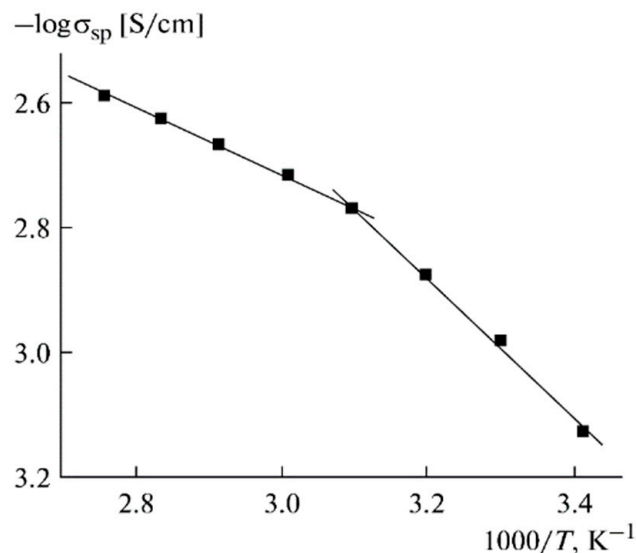

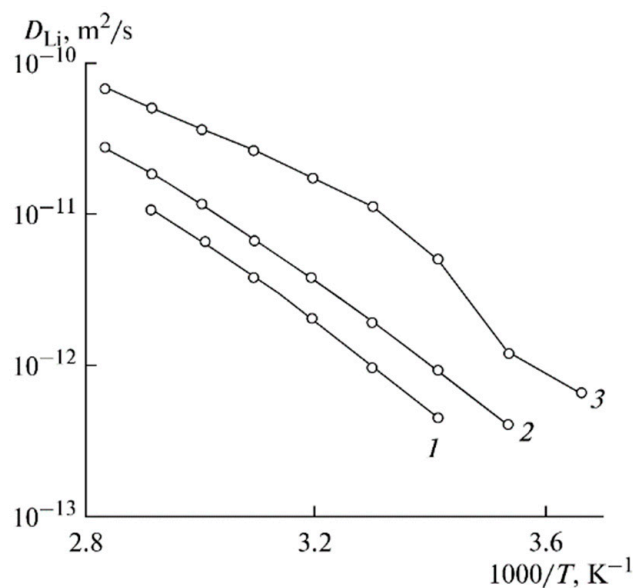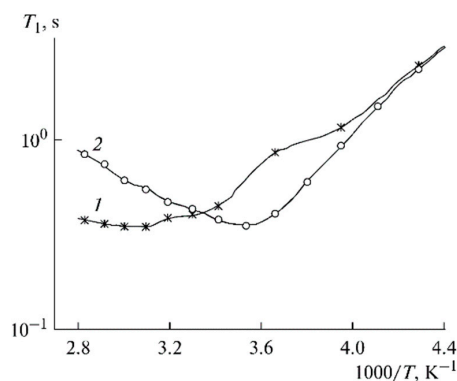**Figure 13.** Temperature dependence of the specific ionic conductivity for PGE no. 9 [53].

Figure 14. Temperature dependences of the Li$^+$ self-diffusion coefficients for PGE no. (**1**) 2, (**2**) 5, and (**3**) 8 [53].

The Arrhenius law approximates these dependences. The temperature dependences of the ionic conductivity are approximated by two linear regions (Figure 13). The self-diffusion coefficients, ionic conductivities, and activation energies are listed in Table 5.

Table 5. Self-diffusion coefficients of lithium D_{Li}, calculated conductivity σ_{NMR}, activation energies of self-diffusion E_{a}, and conduction $E_{\text{a}}(\sigma_{\text{sp}})$ at different ethylene carbonate concentrations [53].

PGE Composition No.	[EC], wt %	[Li⁺]: [EC] in PGE	D_{Li}, cm²/s (30 °C)	σ_{NMR}, S/cm (30 °C)	$E_{\text{a}}(\sigma_{\text{sp}})$, kJ/mol		E_{a} of Self-Diffusion, kJ/mol
					20–50 °C	60–90 °C	50–80 °C
1	-	1:0			62.3 ± 1.7	48.7 ± 3.3	63.6
2	4.3	1.5:1	8.3×10^{-9}	4.42×10^{-5}	81.8 ± 2.2	57.7 ± 4.2	55.9
3	8.3	1:1.4	7.4×10^{-9}	3.70×10^{-5}	72.1 ± 0.4	50.7 ± 2.6	50.7
5	18.4	1:3.4	1.8×10^{-8}	7.71×10^{-5}	47.3 ± 3.0	33.0 ± 1.2	42.8
6	24.0	1:4.7	2.5×10^{-8}	9.75×10^{-5}	45.9 ± 1.4	28.3 ± 1.5	40.4
7	36.4	1:5.8	1.4×10^{-7}	6.41×10^{-4}	26.6 ± 2.1	12.0 ± 1.8	30.0
9	54.8	1:9.0	2.3×10^{-7}	9.59×10^{-4}	20.9 ± 0.9	9.9 ± 0.3	28.5

Local ionic and molecular motion correlation times can be calculated from spin-relaxation of the ^{7}Li and ^{1}H temperature dependences [126]. The temperature dependences of the ^{7}Li spin-lattice relaxation time T_1 for PGE nos. (1) 2 and (2) 9 are shown in Figure 15. These dependences show minimum correspondence to the conditions $\omega\tau_{\text{c}} \approx 1$, where ω is the NMR frequency, and τ_{c} is the correlation time. As shown above, the correlation time τ_{c} is, crudely, an elementary translational jump for a distance comparable with the size of a solvated cation.

Figure 15. Temperature dependences of the ^{7}Li spin-lattice relaxation time T_1 for PGE nos. (**1**) 2 and (**2**) 9 [53].

The temperature dependences of the correlation times are shown in Figure 16.
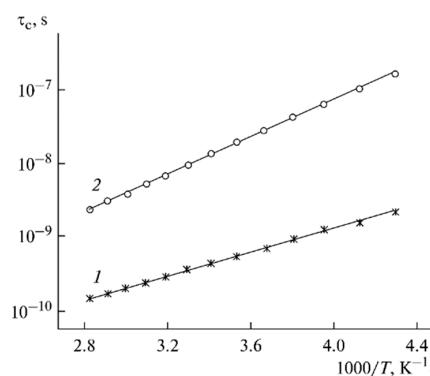
Figure 16. Temperature dependences of the correlation times of ^{7}Li⁺ in PGE nos. (**1**) 2 and (**2**) 9 [53].

Assuming that the size of a solvated cation *l* is about 0.5 nm from the Einstein relationship ($D_{Li} = l^2/6\tau_c$), the calculated values are 1.5×10^{-6} cm^2/s for the sample with the maximum solvent content (no. 9) and 4×10^{-8} cm^2/s for sample no. 2 (minimum EC content).

As follows from Table 5, these values differ by one order of magnitude. This is an acceptable agreement because the estimation of the correlation time is very crude. It may be assumed that the lithium cation macroscopic transfer is controlled by translational jumps over the distances compared with the sizes of solvated cationic complexes.

The dependences of the self-diffusion coefficients of ^{7}Li and ^{1}H are symbate (Figure 17).
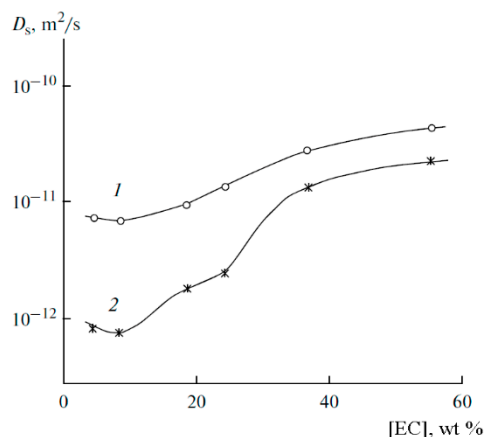
**Figure 17.** Dependences of the average self-diffusion coefficient of ^{1}H (**1**) and self-diffusion coefficient of ^{7}Li$^+$ (**2**) on the solvent concentration [53].

Similarly, the ^{7}Li and ^{1}H spectra contain at least two components (Figure 18), which may be attributed to protons of PEDA and solvent molecules.
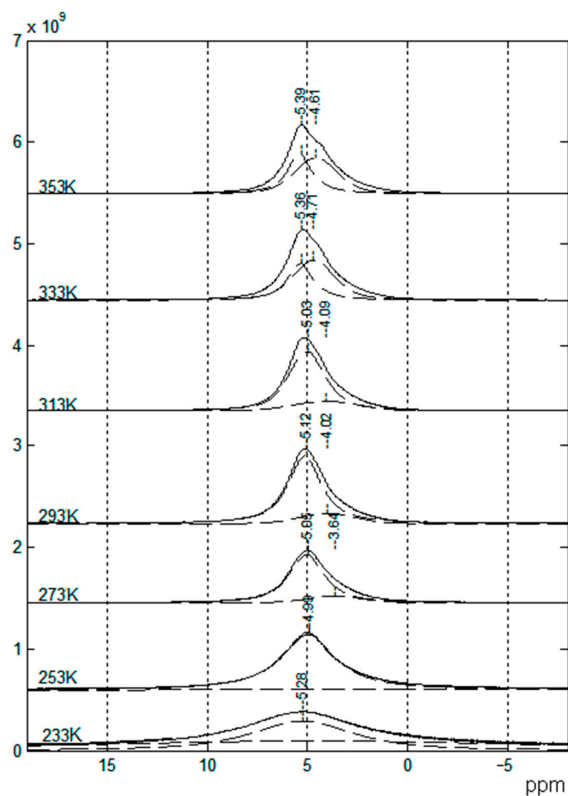
Figure 18. ^{1}H NMR spectra of SPE no. 9 at different temperatures [53].

The NMR spectra of polymer electrolytes are usually not resolved (insertion spectrum in Figure 19). Therefore, a high resolution in the solid magic angle spinning (MAS) technique may be very efficient (well-resolved spectrum in Figure 19). Valuable information concerning polymer electrolyte chemical structure and composition can be obtained from the MAS ^{1}H and ^{13}C NMR spectra. The ^{1}H NMR MAS spectrum of PGE containing 54.8% EC (no. 9, Table 4) is shown in Figure 19.
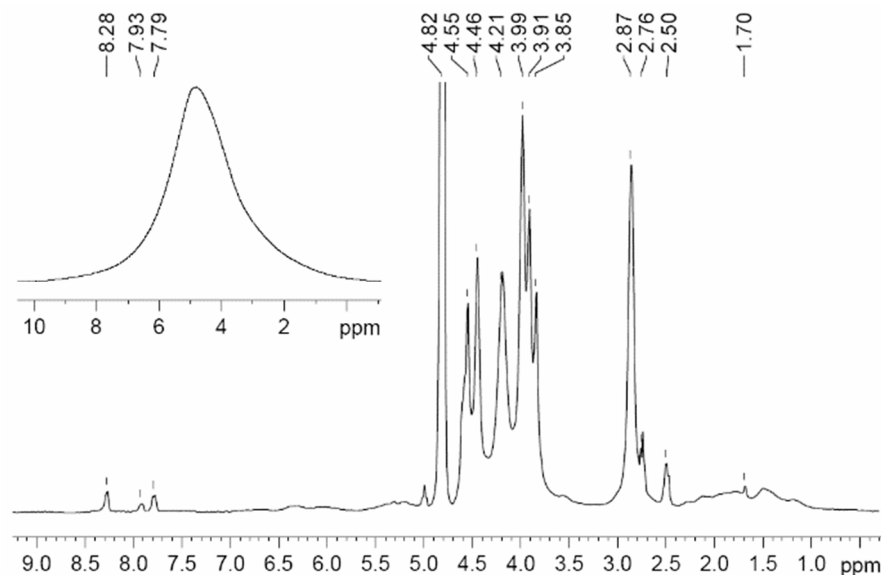

Figure 19. ^{1}H MAS NMR spectrum of PGE containing 54.8 wt % EC (no. 9, Table 1). Chemical shifts were measured relative to ethylene carbonate CH_2 group protons (4.82 ppm relative to TMS). The sample spinning rate is 5 kHz. The ^{1}H NMR spectrum without magic angle spinning is shown in the insert [54]. (δ): 4.82 (br.s, CH_2, EC); 4.46, 2.76 (both br.s, CH_2 and CH_2CO, 2-hydroxyethyl acrylate dimer); 3.99, 2.87 (both br.s, CH_2O and CH_2CO, polymeric units of PEDA); 1–2.50 (br.m, CH and CH_2, cyclic groups of PEDA); 7.79, 8.28, 7.93 (all br.s, NH, $H_2C=CH$, PEDA); 4.20 (br.s, OH, HEA); 3.91, 3.85, 2.50 (br.s, CH_2, HEA).

A decrease in the solvent concentration is accompanied by broadening and weakening of the line of methylene protons of EC (4.82 ppm). Thus, the MAS NMR spectra confirm the chemical structure and composition of the polymer electrolyte.

As mentioned above, the diffusion decay of ^{1}H for the samples containing more than 12 wt % EC is approximated by the sum of three exponential components described by Equation (2): fast (phase 1), medium (phase 2), and slow (phase 3) (Figure 20). The diffusion decays for the samples with a lower EC content show the biexponential shape. No spin echo signal is detected for the solvent-free polymers. The self-diffusion coefficient in phase 3 is almost independent of the solvent content since the samples contain 12 wt % EC (Figure 21, curve 3). The part of phase 3 is close to the ratio of the number of hydrogen atoms in the cyclic dimer of 2-hydroxyethyl acrylate to that in EC. Therefore, the slow component belongs to the molecules of 2-hydroxyethyl acrylate dimer, but the medium and the fast components (phases 1 and 2, respectively) are due to the solvent molecules. As shown in Figure 21, the self-diffusion coefficient of the medium component is close to that of lithium ions. Therefore, the medium component is due to the solvation of Li^+ by EC molecules, while the fast one corresponds to the EC molecules connected to PEDA. These two types of molecules are exchanging, and the exchange time is about several hundreds of ms [54].
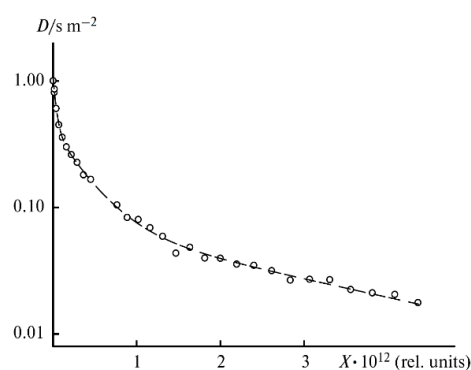
Figure 20. ^{1}H diffusion decay of PGE containing 12% EC wt % (sample 4, Table 1) and its approximation (dashes), $X = \gamma^2 g^2 \delta^2 (\Delta - \delta/3)$ [54].
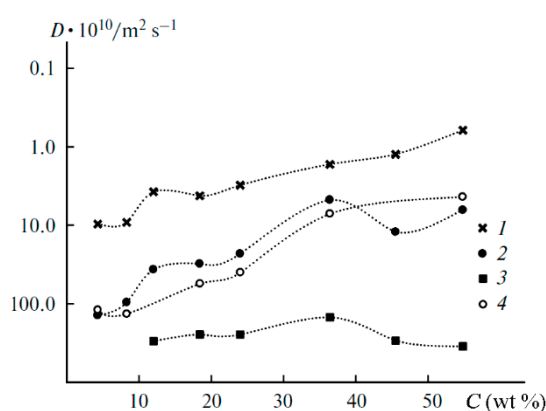
Figure 21. Dependences of the ^{1}H self-diffusion coefficients (*D*) on the solvent concentration (*C*) for the fast (**1**), medium (**2**), and slow (**3**) components; (**4**) is the same for lithium cations [54].

The results of the NMR study of PGE are consistent with the quantum-chemical modeling of PEDA-LiCLO$_4$-EC complexes and the study by IR spectroscopy of the same PGE compositions (Table 1) [53,54].

The density functional theory studies of the energy and structures of mixed Li$^+$ complexes and LiClO$_4$ with EC and PEDA, modeled by oligomers H-((CH$_2$)$_2$COO(CH$_2$)$_2$O)$_n$-CH$_3$ ($n \leq 10$), showed a stronger binding of the lithium-ion with the polymer matrix in the mixed complexes with one EC molecule at a low content of EC. This most likely resulted in a decrease in conductivity.

Less stable mixed complexes with three EC molecules can be formed with an increase in the EC fraction. They become unstable in EC excess because of the transition of the Li$^+$ ions to solvate complexes containing only EC molecules [127]. A similar complex "Li$^+$–4ECs and BF$_4^-$–4ECs solvate-separated ion pair" is shown in Figure 7a [121].

3.4. NMR in Gel Electrolytes with Ionic Liquid

Gel electrolytes with the ionic liquid addition are very perspective. The NMR investigations of these systems are given in [47,50,57–61,128].

Salt LiTFSI, IL 1-butyl-1-methylpyrrolidinium (Pyr$_{14}$) TFSI and a variable amount of poly(ethylene oxide) electrolyte were studied by ^{1}H, ^{7}Li, ^{19}F diffusion NMR and electrophoretic NMR (eNMR). It was shown that, depending on the composition, the mechanism of vehicular Li$^+$ transport via anionic clusters shifts to the chain-dominated transport mechanisms. The lithium transport properties of the electrolytes based on the ionic liquid can be improved by the addition of PEO [50].

The 1-butyl-3-methylimidazolium tetrafluoroborate–propylene carbonate–ethylene carbonate, polyethylene glycol diacrylate polymer electrolyte, and LiBF$_4$ salt system (PGE) were investigated by high resolution and pulsed-field gradient NMR.

The composition and conductivities are given in Table 6 [59].

Table 6. Composition, conductivity (σ), and self-diffusion coefficients (D_s) of PE measured by the PFG ^{7}Li NMR technique.

No.	Ratio of PE Components, mol					σ/S·cm^{-1} (20 °C)	D_1 m^2/s	p_1	D_2, m^2/s	p_2
	PEG DA	LiBF$_4$	BMIBF$_4$	PC	EC					
1	1	1	1	–	–	2.9×10^{-6}	-	-	-	-
2	1	1	2.5	–	–	2.4×10^{-5}	4.5×10^{-12}	1	-	-
3	1	1	6.5	–	–	1.4×10^{-4}	4.8×10^{-12}	1	-	-
4	1	1	2.5	2.2		2.4×10^{-4}	4.5×10^{-13}	0.76	2.2×10^{-11}	0.24
5	1	1	2.5	3.5		6.9×10^{-4}	1.7×10^{-12}	0.89	5.7×10^{-11}	0.11
6	1	1	2.5	5.6		8.5×10^{-4}	2.1×10^{-13}	0.93	6.1×10^{-11}	0.07
7	1	1	5.6	–	3.4	8.1×10^{-4}	2.6×10^{-12}	0.77	2.4×10^{-11}	0.23
8	1	1	4.5	–	5.6	1.2×10^{-3}	4.2×10^{-12}	0.78	2.6×10^{-11}	0.22
9	1	1	6.0	–	9.5	2.5×10^{-3}	1.2×10^{-11}	0.83	4.1×10^{-11}	0.17

As shown in Figure 22, the ^{1}H spectrum of compound 3 contains relatively narrow intense lines corresponding to the BMIBF$_4$ ionic liquid and the broad signals of the PEG-DA polymer: -CH$_2$-C(O)- 1.5–2.5 ppm; -CH$_2$-O- 3.5–4.5 ppm; and -C=CH$_2$ 7–9 ppm.
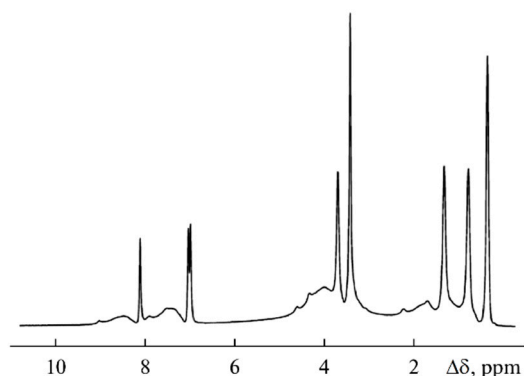
Figure 22. ^{1}H NMR spectra of sample 3 [58].

The ^{7}Li NMR spectra of samples 1–3 are presented in Figure 23. The linewidth decreases from sample 1 (270 Hz) to sample 3 (20 Hz), which indicates that the molecular mobility increases with increasing BMIBF$_4$ content. The linewidth was 100, 30, and 50 for the propylene carbonate addition (samples 4, 5, and 6, respectively). The lines also narrowi with increasing ethylene carbonate addition from 50 to 15 Hz (7–9 samples).
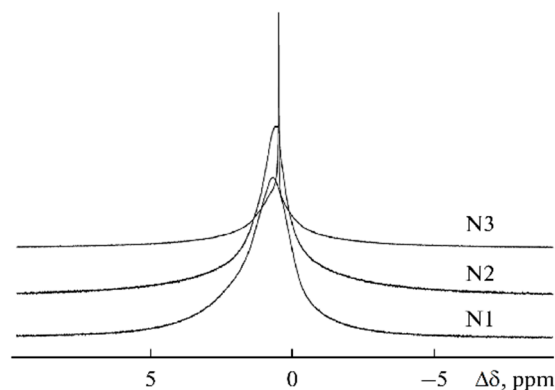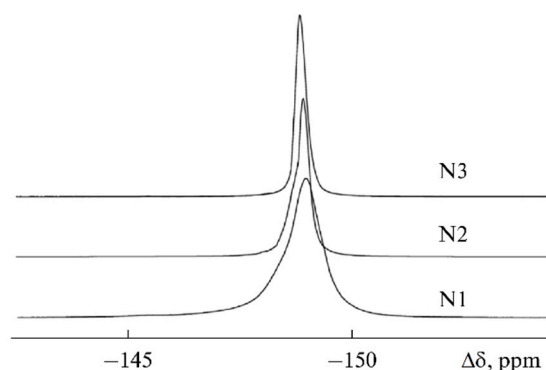

Figure 23. ^{7}Li NMR spectra of samples 1–3 [58].

The diffusion decays were approximated by one or two exponents. The biexponential shape indicates two phases with different self-diffusion coefficients (D_1, D_2) and populations (p_1, p_2) [59].

As shown in Table 6, only one type of Li^+ coordination environment (solvation by the polymer matrix) is observed in the absence of organic solvent. As the 1-buthyl-3-methylimidazolium tetrafluoroborate content in the polymer increases from 44 to 64 wt % (compositions 2 and 3), the self-diffusion coefficients remain unchanged, but the conductivities increase by an order of magnitude. Two phases of lithium ions are formed with the addition of the solvent (compositions 4–9). The phase with the fast Li^+ is likely due to the formation of complexes involving the solvent molecules. When propylene carbonate was added (from 15 to 31 wt % (compositions 4–6)), the conductivity also increased. The highest conductivity was achieved for composition no. 9, where the Li^+ self-diffusion coefficients D_1 and D_2 are of the same order of magnitude: 4.1×10^{-11} and 1.2×10^{-11} m^2/s. This fact indicates the substitution of ethylene carbonate molecules for the units of the polymer matrix in the Li^+ ion coordination [53,127].

The ^{19}F linewidth changed in a similar way (Figure 24). The line narrowed from 350 to 120 Hz for the samples from 1 to 3.

Figure 24. ^{19}F NMR spectra of samples 1–3 [58].

The self-diffusion coefficients of the anions containing ^{19}F are presented in Table 4. As shown in Table 7, for composition 1 without solvent, only one low self-diffusion coefficient (6.1×10^{-13} m^2/s) is observed, and the anions are likely immobilized on the polymer matrix. With an increase in the ionic liquid fraction, highly mobile anions appear with a self-diffusion coefficient of about 10^{-11} m^2/s. With the addition of solvent compounds, the self-diffusion coefficient increased from 6.0×10^{-12} to 2.2×10^{-11} m^2/s (propylene carbonate) and from 8.6×10^{-12} to 3.2×10^{-11} m^2/s (ethylene carbonate). It should be noted that the self-diffusion coefficients of the anions are comparable to those of lithium cations (compositions 4–9) in spite of the fact that the anion size is larger than the cation size. This can be caused by cation solvation by solvent molecules.

Table 7. ^{19}F self-diffusion coefficients [59].

| No.	D_1, m^2/s	p_1	D_2, m^2/s	p_2
1	6.07×10^{-13}	1	–	–
2	7.91×10^{-13}	0.7	1.73×10^{-11}	0.33
3	2.60×10^{-12}	0.63	1.27×10^{-11}	0.39
4	6.00×10^{-12}	1	–	–
5	1.79×10^{-11}	1	–	–
6	2.2×10^{-11}	1	–	–
7	8.57×10^{-12}	1	–	–
8	1.71×10^{-11}	1	–	–
9	3.24×10^{-11}	1	–	–

The network polymer gel electrolyte matrix based on polyethylene glycol diacrylate in a medium of ionic liquid EMIBF$_4$ and LiBF$_4$ with PC and EC was investigated. The polymer compositions are given in Table 8 [60].

Table 8. Compositions, conductivity (σ), and self-diffusion coefficients (D_s) of PE measured by the PFG ^{1}H, ^{7}Li, and ^{19}F NMR technique (T = 24 °C). Ratio PEG DA/LiBF$_4$ =1/1 mol [60,61].

| No.	Ratio of PE Components, mol			σ/S·cm^{-1} (20 °C)	D_s/m^2·s^{-1}		
	EMIBF$_4$	EC	PC		^{1}H	^{7}Li *	^{19}F
1	1	–	–	1.4×10^{-6}	5.8×10^{-13}	2.0×10^{-13}	3.6×10^{-13}
2	2.5	–	–	7.4×10^{-5}	2.5×10^{-12}	5.5×10^{-13}	1.5×10^{-12}
3	6.5	–	–	2.6×10^{-3}	2.5×10^{-11}	5.0×10^{-12}	1.8×10^{-11}
4	6	–	3	2.6×10^{-3}	3.0×10^{-11}	5.2×10^{-12} (0.9) 2.5×10^{-10} (0.1)	2.3×10^{-11}
5	6	–	6	3.6×10^{-3}	4.0×10^{-11}	9.6×10^{-12}	3.6×10^{-11}
6	6	–	9	4.4×10^{-3}	4.4×10^{-11}	1.3×10^{-11}	4.1×10^{-11}
7	6	3	–	2.1×10^{-3}	3.0×10^{-11}	6.1×10^{-12} (0.9), 4.0×10^{-10} (0.1)	2.5×10^{-11}
8	6	6	–	3.9×10^{-3}	3.2×10^{-11}	1.3×10^{-11}	4.2×10^{-11}
9	6	9	–	4.2×10^{-3}	5.1×10^{-11}	1.3×10^{-11}	4.8×10^{-11}

* Phase population with a given D_s is indicated in parentheses.

For polymer electrolytes without solvent, the diffusion decay is characterized by a periodic oscillation of the spin-echo amplitude (beats), which indicates a periodical spatial diffusion restriction (Figure 25). This restriction size is about 3.5 μm. The beats disappeared with increasing ionic liquid content and solvent additions, followed by increasing ^{1}H and ^{19}F self-diffusion coefficients and ionic conductivity by 2–3 orders of magnitude and by an order of magnitude for Li$^+$ cations (Tables 1 and 2).
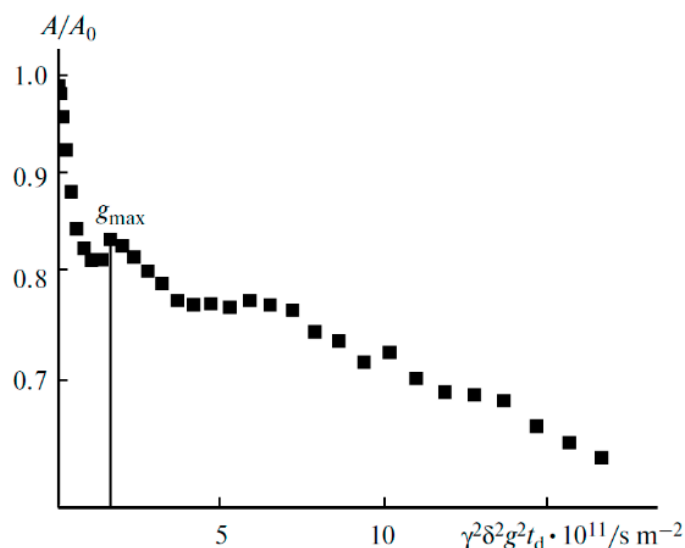
Figure 25. Diffusion decay on ^{7}Li for the composition of PE 1 [60].

Thus, a periodical network is initially formed in the polymer. Ionic liquid insertion decreases the linkage density, and the ionic and molecular mobilities increase. Solvent addition causes further network loosening, and restriction disappears, followed by the exponential diffusion decay (Figure 26). Ionic liquid ions and BF$_4^-$ anions possess the highest mobility.
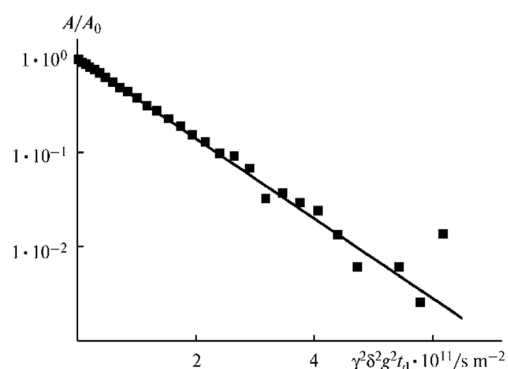
Figure 26. Diffusion decay on ^{7}Li for the composition of PE 5 [60].

Self-diffusion coefficients of ^{7}Li$^+$ cations in the cross-linked polymer gel electrolytes based on PEG DA-EMIBF$_4$-LiBF$_4$ and the sample compositions are given in Table 8 [61]. As shown in Table 8, a small amount of solvent addition (EC and PC) results in phase (10% population) formation with high lithium cation self-diffusion coefficients D_{s2} ($D_{s2} = 4.0 \times 10^{-10}$ m^2/s for sample 7 with EC and 2.5×10^{-10} m^2/s for sample 4 with PC, respectively), which are two orders of magnitude higher than the self-diffusion coefficients D_{s1} of the main population phases. It may be assumed that the fast Li$^+$ diffusion is due to the solvation of EC and PC complexes. At a higher solvent content, we observe the average self-diffusion coefficient as a result of a fast exchange between ^{7}Li located in different environments, which increases with an increasing solvent amount (Table 8).

Lithium and 1-ethyl-3-methylimidazolium tetrafluoroborates (EMIBF$_4$]) in PC solutions were studied by high-resolution ^{1}H, ^{7}Li, ^{11}B, ^{13}C, and ^{19}F NMR. The degree of solvation of Li$^+$ ions was also determined from a pulsed-field gradient ^{1}H, ^{7}Li, and ^{19}F NMR measurements. The structures of Li$^+$ solvation complexes with molecules of propylene carbonate and BF$_4^-$ anions and complexes associated with the ionic liquid were calculated using the density-functional theory. The calculated and experimental chemical shifts were compared. The structures of the complexes are shown in Figures 27 and 28.
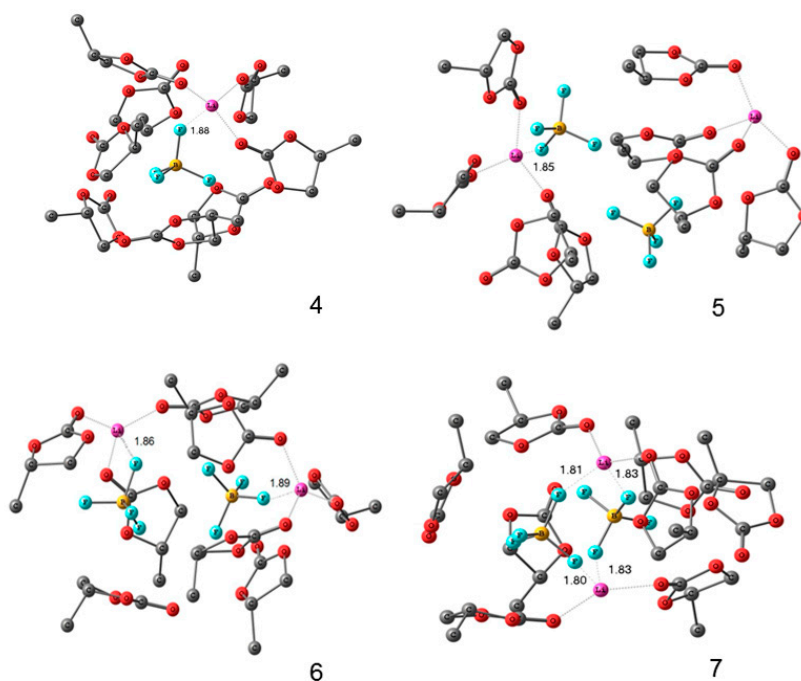
Figure 27. Calculated structures of the solvation complexes without ionic liquid components. Hydrogen atoms are omitted. Interatomic distances are given in Å [128].
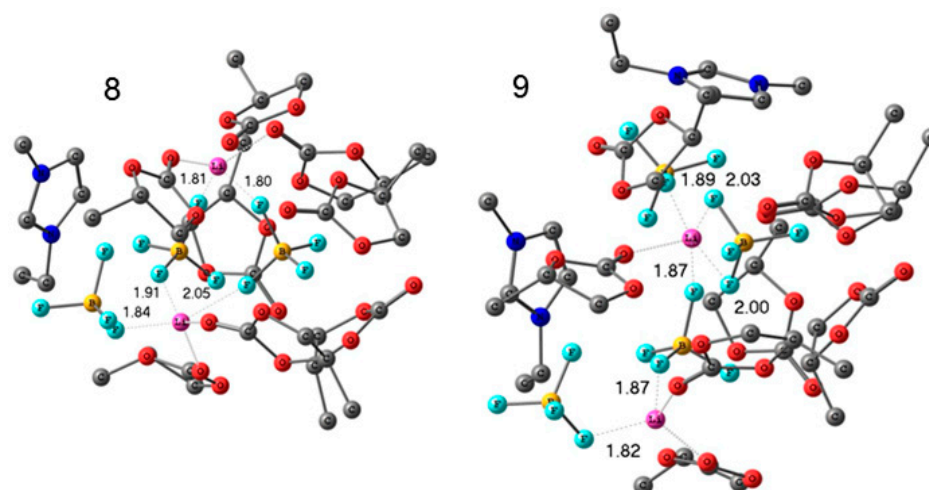
Figure 28. Calculated structures of the solvation complexes with the IL components. Hydrogen atoms are omitted. Interatomic distances are given in Å [128].

3.5. NMR in Nanocomposite Polymer Electrolytes

NMR studies in nanocomposite polymer electrolytes were considered in [49,65,72,73, 77,92,101,104–106].

The mobility of the molecules containing [7]Li and ^{19}F was measured by pulsed-field gradient NMR and spin-lattice relaxation techniques in composite gel polymer electrolytes based on organo-modified montmorillonite clays. It was shown that the smectite clay surfaces solvate lithium and triflate ions, creating a preferential ion conduction pathway [49].

Solid-state ^{7}Li NMR of a PCL-PTMC copolymer shows fast Li ions for the [7]Li−[7]Li exchange between the phases of the polymer electrolyte LLZO compared to the PEO-based composite [133].

Two Li^+-insulating oxide (fluorite $Gd_{0.1}Ce_{0.9}O_{1.95}$ and perovskite $La_{0.8}Sr_{0.2}Ga_{0.8}$-$Mg_{0.2}O_{2.55}$) polymer composite electrolytes were investigated by Li solid-state NMR. An increase in the Li+ ion (>10%) population results in a more mobile fraction in the composite electrolytes. This increase results from a strong interaction between the O_2^- of the Li anions of the salt and oxygen of the surface oxide vacancies [73].

In poly(ethylene carbonate) and Li bis(fluorosulfonyl) imide, the influence of TiO_2 nanoparticles on Li^+ mobility was observed. The maximum values of Li^+ self-diffusion and transport numbers were about 10^{-11} m^2/s and 0.8, respectively, in the composites containing 1 wt % nanoparticles [101]. The highly conductive phase $LiBH_4$, LiI with Al_2O_3 addition was investigated by ^{1}H, [6]Li, ^{7}Li, ^{11}B, and ^{27}Al NMR [104]. An interaction of $LiBH_4$-LiI with Al was shown by ^{27}Al MAS NMR [105,106].

^{7}Li NMR spectroscopy was applied to characterize the ion dynamics in quaternary composite solid-state electrolytes. The temperature dependences of the diffusion coefficients show two components consistent with the change in the morphology near the transition temperature where crystallinity was varied [77].

It was suggested based on ^{1}H and ^{7}Li NMR that the high ionic conductivity (0.5 mS/cm) and low activation energy (2.3 kJ/mol) of ion transport are due to grain boundaries between an excess of LiI and inert $LiAlO_2$ ceramic nanoparticles in the composite polymer in the ceramic electrolytes [72].

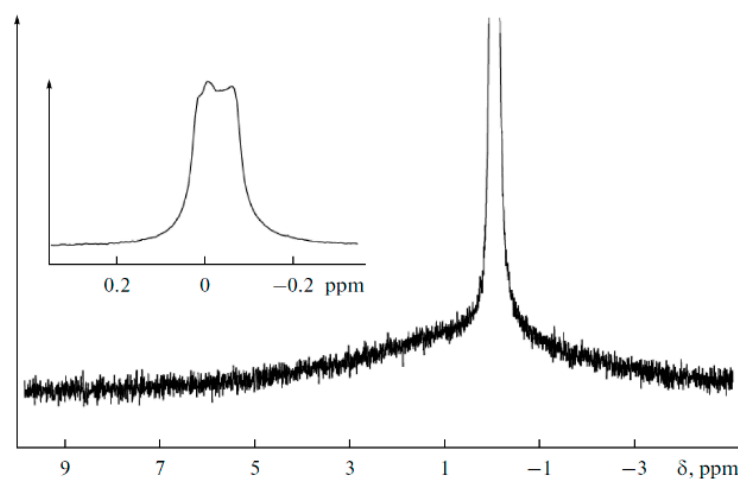The NMR study of the nanocomposite polymer electrolytes is discussed in detail below.

The effects of TiO_2 (~60 nm) and Li_2TiO_3 (~20 nm) nanoparticles on the structure, conductivity, and self-diffusion in the polyether diacrylate–$LiClO_4$–ethylene carbonate polymer gel electrolytes were studied. The compositions of the polymer electrolytes with nanoparticles additions are given in Table 9.

Table 9. Compositions of the polymer electrolytes added with nanoparticles [92].

No. of Polymer Electrolyte	Polymer Electrolyte Initial Components, wt %			
	PEDA:EC (1:1)	LiClO$_4$	Nanodisperse Filler	Benzoyl Peroxide
1	91.1	7.5	–	1.4
2	81.1	7.5	TiO$_2$—10.0	1.4
3	81.1	7.5	Li$_2$TiO$_3$—10.0	1.4

The ^{7}Li NMR spectrum for the polymer electrolyte with Li$_2$TiO$_3$ (no. 3) is shown in Figure 29. The narrow line is a lithium perchlorate signal, while wide pedestals are due to lithium from nanoparticles. The narrow line consists of two lines attributed to different lithium positions (insert in Figure 29). The narrow line without splitting is observed for the polymer electrolyte with TiO$_2$ addition.

Figure 29. MAS ^{7}Li NMR spectrum of the nanocomposite polymer electrolyte added with Li$_2$TiO$_3$. The sample spinning frequency is 10 kHz [92].

In polymer electrolyte no. 3 (Li$_2$TiO$_3$ addition), the exponential diffusion decay of ^{7}Li is observed, which is characterized by only one self-diffusion coefficient (6.4×10^{-12} m^2/s, Figure 30).
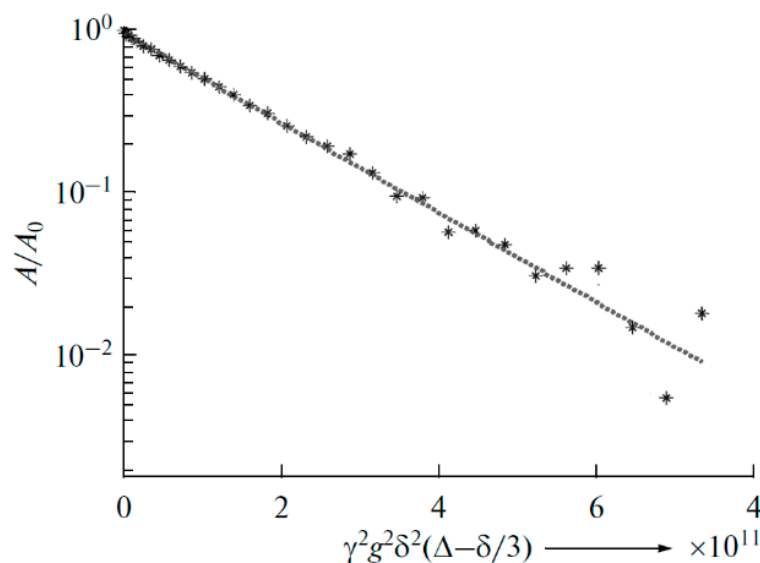
Figure 30. Diffusion decay of ^{7}Li for polymer electrolyte no. 3 with Li$_2$TiO$_3$ nanoparticles (10 wt %) [92].

For the polymer electrolyte with the addition of TiO_2 nanoparticles, the biexponential diffusion decay of ^7Li was recorded, which indicates two lithium surroundings or phases (Figure 31). The partial self-diffusion coefficients are 1.2×10^{-11} and 1.7×10^{-12} m^2/s, and the phase populations are 0.9 and 0.1, respectively.
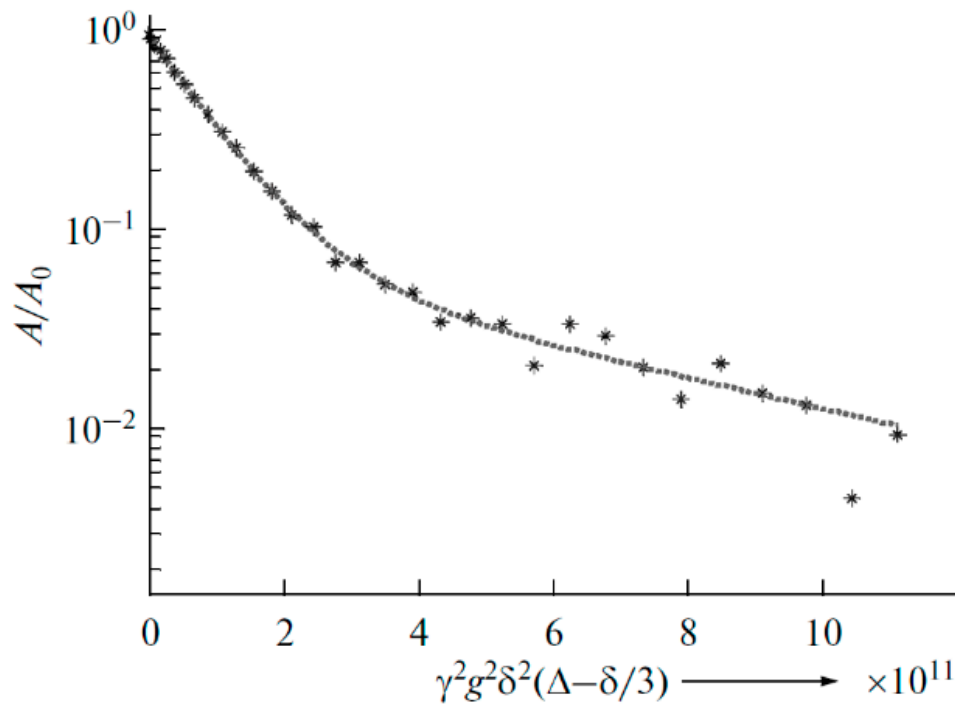
Figure 31. Diffusion decay of ^7Li for polymer electrolyte no. 2 with TiO_2 nanoparticles (10 wt %) [92].

Some peculiarities of ion transport in the nanocomposite system based on a network matrix synthesized by radical polymerization of polyethylene glycol diacrylate in the presence of liquid aprotic electrolyte containing 1 M $LiBF_4$ in γ-butyrolactone and SiO_2 nanopowder were revealed. The compositions of the polymer electrolytes are given in Table 10.

Table 10. Parameters of ion transport for different NPE compositions: conductivity (σ_{sp}) at 20 °C, effective activation energies of conduction (E^{ef}_a (σ_{sp})), self-diffusion coefficients (D_s), and transport numbers with respect to lithium cations (t_+) [65].

No.	Starting Components of NPE, wt %				t_+	D_s, 10^{-10} m^2/s (24 °C)	σ, mS/cm (20 °C)
	PEG-DA$_{575}$	1 M LiBF$_4$ in GBL	SiO$_2$	BP			
1	15	84	0	1	0.44	1.10	3.24
2	15	82	2	1	0.49	1.20	3.76
3	15	80	4	1	0.34	0.83	3.35
4	15	78	6	1	0.32	0.76	4.52
5	15	76	8	1	0.29	0.73	2.61
6	15	74	10	1	–	0.61	2.34

As shown in Figure 32, spin-echo ^7Li attenuations (diffusion decays) are approximated by Equation (1). Therefore, lithium cation diffusion is characterized by only one self-diffusion coefficient.
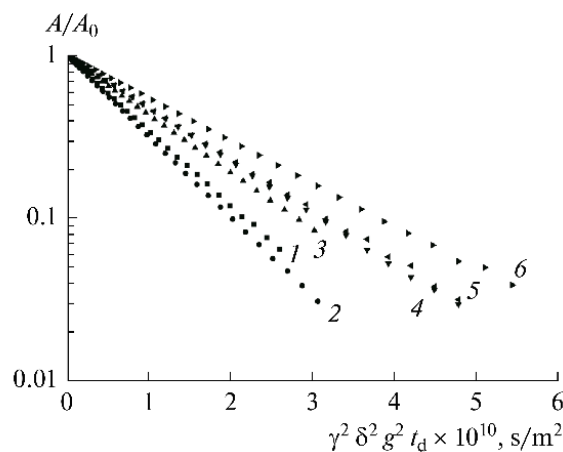
Figure 32. Dependence of amplitudes of spin-echo signals of ^{7}Li on the squared amplitude of magnetic field gradient pulse (diffusion decay). The numbers correspond to the electrolyte composition numbers (Table 10) [65].

Lithium-ion self-diffusion coefficients D_s and ionic conductivities σ depend on the SiO$_2$ content in the electrolyte (Table 10).

The highest self-diffusion coefficient (1.2×10^{-10} m^2/s) corresponds to 2 wt % SiO$_2$. This composition also shows the highest transport number of lithium cations (0.49). An increase in the number of mobile charge carriers is very likely due to salt dissociation. The second maximum of conductivity at 6 wt % SiO$_2$ (no. 4) of the nanopowder content may be explained by the contribution of nanoparticle packing and the formation of additional pathways favorable for ion transport.

The scheme of ionic transport is given in Figure 33.
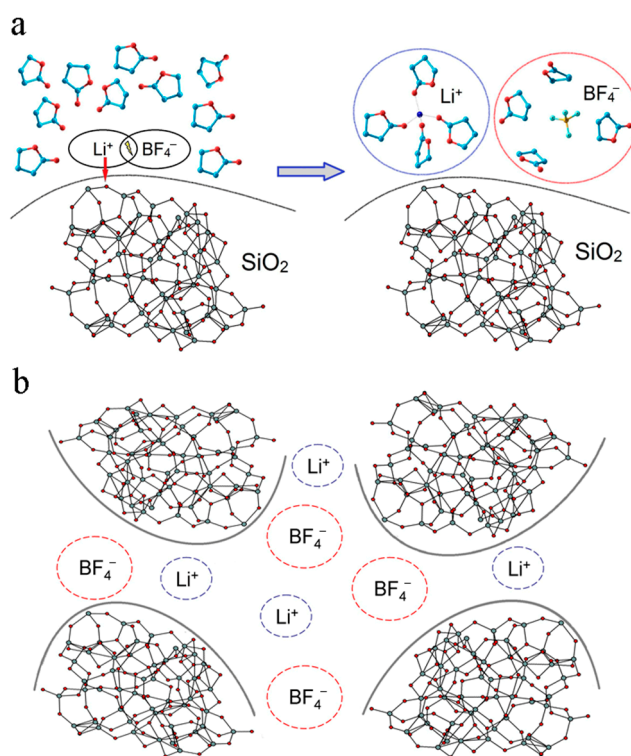
Figure 33. Scheme of ionic transport in the nanocomposite polymer electrolyte: (**a**) mechanism of LiBF$_4$ salt dissociation to ions involving SiO$_2$ surface groups; (**b**) ion transport over the surface of nanoparticles. Solvate shells of ions and ion pairs are designated by oblong dashed circles [65].

3.6. Nuclear Magnetic Resonance Study of Sodium-Ion Electrolytes

Batteries involving sodium salts are desirable because they are readily available at a low cost. On the one hand, ^{23}Na NMR spectroscopy should be more sensitive to Na+ cation surroundings because the sodium nuclear chemical shift varies in some tenth ppm compared to [7]Li chemical shift variations (1–2 ppm). On the other hand, the spin-spin relaxation time of [23]Na is short and, therefore, it is difficult to measure the self-diffusion coefficient by pulsed-field gradient NMR. At the present time, only some papers are devoted to ^{23}Na NMR in polymer electrolytes.

LiPF$_6$ and NaPF$_6$ salts solutions in glycol dimethoxy ethers (glymes) were studied [134,135]. The self-diffusion coefficients for [7]Li, [23]Na, and ^{19}F in monoglyme (G1), diglyme (G2), and tetraglyme (G4) decrease from 10^{-9} m^2/s in G1 to 10^{-11} m^2/s in G4 [134]. The conductivities calculated from the Nernst–Einstein equation were compared with the measured values, and the degree of ion association was determined. The electrolytes show ion pairing with increasing temperature, which is explained by decreasing solvent dielectric constant with temperature. It was shown that ion association decreases if the solvent molecular size increases. The self-diffusion coefficients of ^{1}H, ^{19}F, and [23]Na of NaCF$_3$SO$_3$ solutions in dimethoxyethane (DME) and diethylene glycol dimethyl ether (DEGDME) were measured by PFG NMR [135]. The temperature dependences of DH, DF, and DNa self-diffusion coefficients and sodium transport number (t_+) calculated from the self-diffusion coefficients are shown in Figure 34. The DME and DEGDME electrolytes show suitable characteristics for sodium batteries, where the ion conductivity is about 10^{-3} S/cm, but the sodium transport number is 0.5. A DEGDME solution is more suitable for sodium battery applications
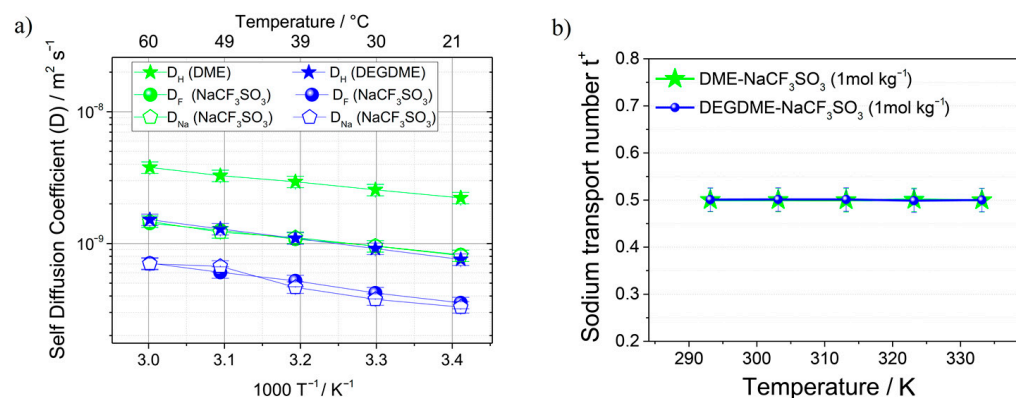
Figure 34. (**a**) Self-diffusion coefficients of ^{1}H, ^{19}F and [23]Na in the DME-NaCF$_3$SO$_3$ (1 mol/kg) and DEGDME-NaCF$_3$SO$_3$ (1 mol/kg) electrolytes determined from 20 °C to 60 °C by PFG-NMR. (**b**) Sodium transport number (t_+) calculated from the self-diffusion coefficients measured by PFG-NMR [135].

The PAMAM (Poly(amidoamine)) dendrimers dissolved in propylene carbonate (PC) together with LiTFSI or NaTFSI salts were studied by PFG ^{7}Li, ^{19}F and ^{23}Na NMR [136]. The dependences of the self-diffusion coefficients on temperature and PAMAM content were analyzed. The temperature dependences of PC, [7]Li, ^{19}F and PC, [23]Na, and ^{19}F self-diffusion coefficients for LiTFSI and NaTFSI solutions without PAMAM are shown in Figure 35.
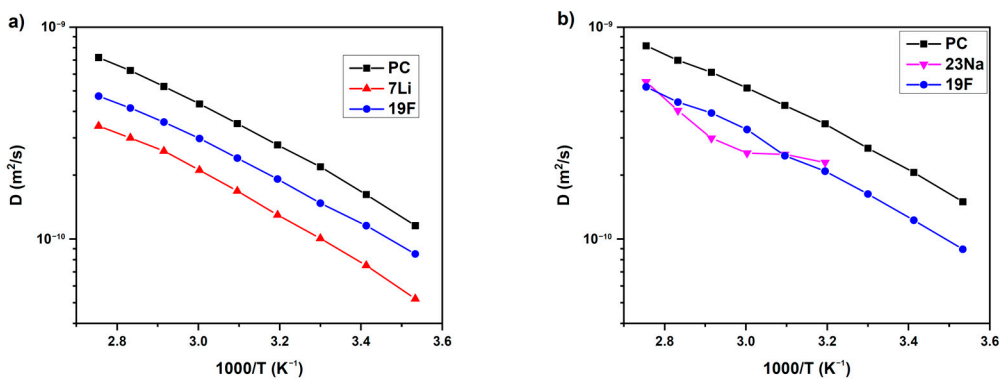
Figure 35. Temperature dependences of the NMR self-diffusion coefficients for the LiTFSI-0%G (**a**) and NaTFSI-0%G (**b**) electrolytes (without PAMAM). Solid lines are guides for the eye [136].

The effect of PAMAM on the diffusivity of Li$^+$ cation (a), TFSI$^-$ anion (b), PC molecules (c), and PAMAM molecules (d) in LiTFSI containing electrolytes is demonstrated in Figure 36.
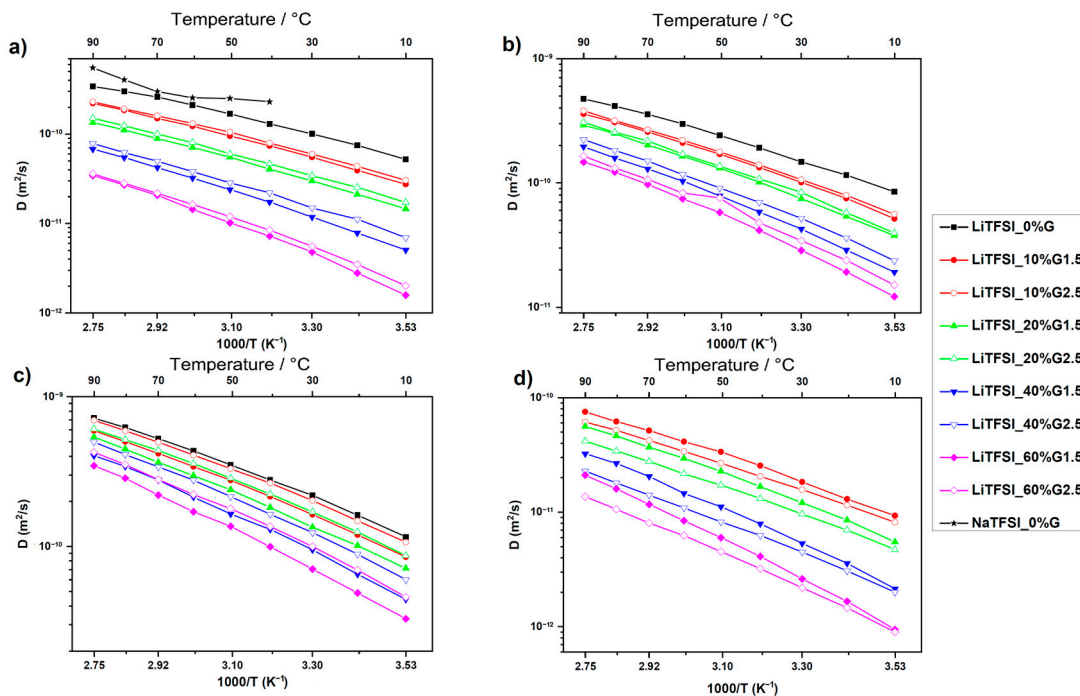
Figure 36. Temperature dependences of the NMR self-diffusion coefficients for the LiTFSI-based electrolytes for Li cation (**a**), TFSI anion (**b**), PC molecules (**c**), and PAMAM molecules (**d**). Solid lines are guides for the eye [136].

The self-diffusion coefficients decrease by orders of magnitude with an increase in the PAMAM content due to increased viscosity. The self-diffusion coefficients of the solvent, cations, and anions are slightly higher in the samples with a high PAMAM generation, which is explained by weaker interactions of the PAMAM dendrimer with the cations, anions, and PC or a poor penetration of a solution into PAMAM G2.5 compared to PAMAM G1.5. A decrease in the Li cation self-diffusion coefficient compared with the TFSI$^-$ anion and PC is observed. The diffusion of lithium cations is slower than that of a large anion. The TFSI lithium self-diffusion coefficient decreases with an increase in the concentration of PAMAM because of cation–dendrimer interactions.

4. Conclusions

The first significant half of the review (Section 2) is devoted to the compositions and conductivity of various types of electrolytes for lithium-ion batteries developed over the past decade. The compositions and conductivity of liquid electrolytes and solid, gel, and nanocomposite polymer electrolytes are considered in the second part of the review.

First, the compositions and conductivity of the liquid electrolytes are considered. The conduction mechanisms in the polymer gel electrolytes that contain them should be understood. Ion transport occurs through the liquid phase in gel systems.

Second, the compositions and conductivity of the solid polymer electrolytes are briefly considered. Gel electrolytes are discussed in the next section. They compose the most considered class of polymer electrolytes. They contain both aprotic solvents and ionic liquids. In the last paragraph, the nanocomposite electrolytes have found consideration. Here it is necessary to distinguish the composition of the polymer–salt–nanoparticle and polymer–salt–nanoparticle–solvent.

NMR applications for the polymer electrolytes are described in the third part.

High-resolution solid-state NMR, especially magic angle spinning (MAS) NMR, NMR relaxation, and pulsed-field gradient NMR applications for ion coordination and mobility, are discussed. Primary attention is given to gel electrolytes.

Section 3.1 is devoted to solid-state NMR, pulse field gradient NMR, exchange spectroscopy, cross-polarization, and rotational echo double-resonance applications to characterize the molecular structure and dynamics in solid polymer and hybrid electrolytes.

In Section 3.2, solutions of $LiBF_4$ and $LiClO_4$ in ethylene carbonate (EC) were studied as model systems by high-resolution ^1H, ^7Li, ^{11}B, ^{13}C, ^{17}O, and ^{35}Cl NMR spectroscopy. The dependence of the multinuclear chemical shifts on the solution concentration was analyzed. The quantum-chemical calculations of nuclear chemical shifts were performed. The structure models of cation-anion-solvent complexes depending on the concentration were proposed on the basis of the comparison of the experimental and calculated chemical shifts. Some examples of complex structures are shown in Figures 6 and 7.

In Section 3.3, these electrolytes in the polymer network are discussed. In a polyester diacrylate (PEDA)–solvent system, two ^7Li NMR lines were observed, and their chemical shifts and widths depended on the EC content. It was concluded that the narrow line was due to mobile Li^+ coordinated by EC molecules, and the wide line belonged to Li^+ that interacted with the polymer matrix. The ^7Li NMR spectra of the composite electrolyte gel, poly(vinylidene fluoride-*co*-hexafluoropropylene) with the addition of silicate aerogel (SAG), ethylene carbonate, and propylene carbonate as solvents at different contents of aerogel and $LiClO_4$, were analyzed. It may be concluded that Li^+ cations interact with SAG, solvent, and PVDF-HPF. These interactions could favor the formation of transport conditions for the fast movement of Li^+ cations over the SAG particles' surface. The ion and solvent mobility in different spatial scales was investigated by NMR relaxation and pulsed-field gradient NMR techniques. It was assumed that the lithium cation macroscopic transfer is controlled by translational jumps over the distances compared with the sizes of the solvated cationic complexes. The comparison of the ionic conductivity calculated from the diffusion coefficient σ_{NMR} using the Nernst–Einstein equation with the experimental conductivity σ_{sp} enables the degree of dissociation α to be calculated as the ratio $\alpha = \sigma_{sp}/\sigma_{NMR}$. The density functional theory studies of the energy and structures of mixed Li^+ complexes and $LiClO_4$ with EC and PEDA, which were modeled by oligomers $H-((CH_2)_2COO(CH_2)_2O)_n-CH_3$ ($n \leq 10$), showed a stronger binding of the lithium ions with the polymer matrix in the mixed complexes with one EC molecule at a low content of EC resulting, most likely, in a decrease in the conductivity. Less stable mixed complexes with three EC molecules can be formed with an increase in the EC fraction. They become unstable in EC excess because of the transition of the Li^+ ions to solvate complexes containing only EC molecules. A similar complex "Li^+–4ECs and BF_4^-–4ECs solvate-separated ion pair" is shown in Figure 7a.

Gel electrolytes with the addition of ionic liquid and nanoparticles are very perspective. In Section 3.4, the 1-butyl-3-methylimidazolium tetrafluoroborate–propylene carbonate–ethylene carbonate, polyethylene glycol diacrylate polymer electrolyte and LiBF$_4$ salt system (PGE) studied by high resolution and pulsed-field gradient NMR are described. Lithium and 1-ethyl-3-methylimidazolium tetrafluoroborates (EMIBF$_4$]) in PC solutions were investigated by high-resolution ^{1}H, ^{7}Li, ^{11}B,^{13}C, and ^{19}F NMR. The degree of solvation of Li$^+$ ion was also determined from pulsed-field gradient ^{1}H, ^{7}Li, and ^{19}F NMR measurements. Only one type of Li$^+$ coordination environment (solvation by the polymer matrix) is observed in the absence of organic solvent. As the 1-buthyl-3-methylimidazolium tetrafluoroborate content in the polymer increases, the self-diffusion coefficients remain unchanged, but the conductivities increase by order of magnitude. Two phases of lithium ions are formed with the addition of the solvent. The phase with fast Li$^+$ is likely due to the formation of complexes involving the solvent molecules. The anions containing ^{19}F for the composition without solvent are characterized by a low self-diffusion coefficient (6.1×10^{-13} m^2/s), and the anions are likely immobilized by the polymer matrix. When the fraction of the ionic liquid increases, highly mobile anions appear with self-diffusion coefficients of about 10^{-11} m^2/s. It should be noted that the self-diffusion coefficients of the anions are comparable to those of lithium cations despite the anion size, which is larger than the cation size. This can be due to cation solvation by solvent molecules.

The structures of the Li$^+$ solvation complexes with molecules of propylene carbonate and BF$_4^-$ anion and complex associated with the ionic liquid were calculated using the density-functional theory. The calculated and experimental chemical shifts were compared. The structures of the complexes are shown in Figures 27 and 28.

In Section 3.5, the gel polymer electrolyte compositions with nanoparticles are considered. The effects of TiO$_2$ (~60 nm) and Li$_2$TiO$_3$ (~20 nm) nanoparticles on the structure, conductivity, and self-diffusion in the polyether diacrylate–LiClO$_4$–ethylene carbonate polymer gel electrolytes were studied. For the polymer electrolyte with TiO$_2$ nanoparticles, the biexponential diffusion decay of ^{7}Li was recorded, which indicates two lithium surroundings or phases. Ion transport particularities in the nanocomposite system based on a network matrix synthesized by radical polymerization of polyethylene glycol diacrylate in the presence of the liquid aprotic electrolyte containing 1 M LiBF$_4$ in γ-butyrolactone and SiO$_2$ nanopowder were revealed. The self-diffusion coefficients D_s of lithium ions and ionic conductivities σ depend on the SiO$_2$ content in the electrolyte. The highest self-diffusion coefficient (1.2×10^{-10} m^2/s) corresponds to 2 wt % SiO$_2$. This composition also shows the highest transport number of lithium cations (0.49). An increase in the number of mobile charge carriers is very likely due to salt dissociation. The second maximum of the conductivity at 6 wt % SiO$_2$ of the nanopowder content can be explained by the contribution of nanoparticle packing and the formation of additional pathways favorable for ion transport. The scheme of ionic transport is given in Figure 33.

In Section 3.6, some results of the NMR study of sodium ion electrolytes are briefly presented. It was demonstrated that ^{23}Na NMR is very informative for investigating these systems.

Abbreviation:

NaTf	sodium trifluoromethanesulfonate
NaTFSI	sodium bis(trifluoromethanesulfonyl) imide $NaN(SO_2CF_3)_2$
LiTFSI	lithium bis(trifluoromethanesulfonyl) imide$LiN(SO_2CF_3)_2$
LiTf	Lithiumtrifluoromethanesulfonate—$LiSO_3CF_3$
LiBOB	Lithium bisoxalato borate
$BMICF_3SO_3$	1-butyl-3-methylimidazolium trifluoromethanesulfonate
$BMIBF_4$	1-butyl-3-methylimidazolium tetrafluoroborate
$EMIBF_4$	1-ethyl-3-methylimidazolium tetrafluoroborate
[N4441] [TFSI]	tributyl methyl ammonium bis(trifluoromethanesulfonyl)imide
[P4441] [TFSI]	tributyl methyl phosphoniumbis(trifluoromethanesulfonyl)imide
$[Pyr_{14}]PF_6$	1-butyl-1-methyl-pyrrolidinium hexafluorophosphate
$Pyr_{13}TFSI$	N-Propyl-N-methylpyrrolidinium bis(trifluoromethanesulfonyl)imide
$Pyr_{14}TFSI$	N-butyl-N-methyl-pyrrolidinium bis(trifluoromethanesulfonyl) imide
BEMA	bisphenol A ethoxylatedimethacrylate
CD	cyclodextrin
DEC	diethyl carbonate
DMC	dimethyl carbonate
DME	1,2-dimethyl ether
EC	ethylene carbonate
EMC	ethyl methyl carbonate
GBL	gamma-butyrolactone
HBP	hyperbranched polymer based on methyl methacrylate and triethylene glycol dimethacrylate
IL	ionic liquid
IBN	isobutyronitrile
LE	liquid electrolyte
LIB	lithium ion battery
MATEMP	di(2-methylacryloyltrioxyethyl) methyl phosphonate
MTBE	*tert*-butyl methyl ether
NMR	Nuclear magnetic resonance
NPE	Nanocomposite polymer electrolyte
PFG NMR	Pulsed field gradient NMR
PAN	polyacrylonitrile
PAMAM	poly(amidoamine)
PBO	poly [benzyl methacrylate-co-oligo (ethylene glycol) ether methacrylate)]
PC	propylene carbonate
PE	polyethylene
PEDA	polyether diacrylate
PEG	polyethylene glycol
PEG-DA	poly(ethylene glycol) diacrylate
PEG-MA	poly(ethylene glycol) methacrylate
PEG-MEM	poly(ethylene glycol) methyl ether methacrylate
PEMA	poly(ethyl methacrylate)
PEO	polyethylene oxide
xPTHF	poly(tetrahydrofuran)
PGE	polymer gel electrolyte
PMMA	poly(methyl methacrylate)
P(MMA-*co*-BA)	poly(methyl methacrylate-*co*-butylacrylate)
PP	polypropylene
c-PPO	poly [diemethyl-p-vinyl benzyl phosphonate-co-oligo (ethylene glycol) methacrylate] co-polymer
PPO	poly (propylene oxide)
PVC	poly (vinyl chloride)

PVA	polyvinyl alcohol
PVDF	poly(vinylidene fluoride)
PVDF-HFP	poly(vinylidene fluoride-*co*-hexafluoropropylene)
PVS	polyvinylstyrene
SAG	silicate aerogel
SDC	Self-diffusion coefficients
SPE	Solid polymer electrolyte
THF	tetrahydrofuran
TMAN	trimethyl acetonitrile

References

1. Rollo-Walker, G.; Malic, N.; Wang, X.; Chiefari, J.; Forsyth, M. Development and Progression of Polymer Electrolytes for Batteries: Influence of Structure and Chemistry. *Polymers* **2021**, *13*, 4127. [CrossRef] [PubMed]
2. Pigłowska, M.; Kurc, B.; Galiński, M.; Fuć, P.; Kamińska, M.; Szymlet, N.; Daszkiewicz, P. Challenges for Safe Electrolytes Applied in Lithium-Ion Cells—A Review. *Materials* **2021**, *14*, 6783. [CrossRef] [PubMed]
3. Hwang, J.-Y.; Myung, S.-T.; Sun, Y.-K. Sodium-Ion Batteries: Present and Future. *Chem. Soc. Rev.* **2017**, *46*, 3529–3614. [CrossRef] [PubMed]
4. Nayak, P.K.; Yang, L.; Brehm, W.; Adelhelm, P. From Lithium-Ion to Sodium-Ion Batteries: Advantages, Challenges, and Surprises. *Angew. Chem. Int. Ed.* **2018**, *57*, 102–120. [CrossRef]
5. Wang, Y.; Song, S.; Xu, C.; Hu, N.; Molenda, J.; Lu, L. Development of Solid-State Electrolytes for Sodium-Ion Battery—A Short Review. *Nano. Mater. Sci.* **2019**, *1*, 91–100. [CrossRef]
6. Karuppasamy, K.; Theerthagiri, J.; Vikraman, D.; Yim, C.-J.; Hussain, S.; Sharma, R.; Maiyalagan, T.; Qin, J.; Kim, H.-S. Ionic Liquid-Based Electrolytes for Energy Storage Devices: A Brief Review on Their Limits and Applications. *Polymers* **2020**, *12*, 918. [CrossRef]
7. Sultana, S.; Ahmed, K.; Jiwanti, P.K.; Wardhana, B.Y.; Shiblee, M.N.I. Ionic Liquid-Based Gels for Applications in Electrochemical Energy Storage and Conversion Devices: A Review of Recent Progress and Future Prospects. *Gels* **2021**, *8*, 2. [CrossRef]
8. Ray, A.; Saruhan, B. Application of Ionic Liquids for Batteries and Supercapacitors. *Materials* **2021**, *14*, 2942. [CrossRef]
9. Boaretto, N.; Meabe, L.; Martinez-Ibañez, M.; Armand, M.; Zhang, H. Review—Polymer Electrolytes for Rechargeable Batteries: From Nanocomposite to Nanohybrid. *J. Electrochem. Soc.* **2020**, *167*, 70524. [CrossRef]
10. Yarmolenko, O.V.; Yudina, A.V.; Khatmullina, K.G. Nanocomposite Polymer Electrolytes for the Lithium Power Sources (a Review). *Russ. J. Electrochem.* **2018**, *54*, 325–343. [CrossRef]
11. Yao, P.; Yu, H.; Ding, Z.; Liu, Y.; Lu, J.; Lavorgna, M.; Wu, J.; Liu, X. Review on Polymer-Based Composite Electrolytes for Lithium Batteries. *Front. Chem.* **2019**, *7*, 522. [CrossRef] [PubMed]
12. Zhou, D.; Shanmukaraj, D.; Tkacheva, A.; Armand, M.; Wang, G. Polymer Electrolytes for Lithium-Based Batteries: Advances and Prospects. *Chem* **2019**, *5*, 2326–2352. [CrossRef]
13. Munoz, S.; Greenbaum, S. Review of Recent Nuclear Magnetic Resonance Studies of Ion Transport in Polymer Electrolytes. *Membranes* **2018**, *8*, 120. [CrossRef] [PubMed]
14. Fan, X.; Wang, C. High-Voltage Liquid Electrolytes for Li Batteries: Progress and Perspectives. *Chem. Soc. Rev.* **2021**, *50*, 10486–10566. [CrossRef]
15. Quartarone, E.; Mustarelli, P. Review-Emerging Trends in the Design of Electrolytes for Lithium and Post-Lithium Batteries. *J. Electrochem. Soc.* **2020**, *167*, 50508. [CrossRef]
16. Xu, K. Electrolytes and Interphases in Li-Ion Batteries and Beyond. *Chem. Rev.* **2014**, *114*, 11503–11618. [CrossRef]
17. Shestakov, A.F.; Yudina, A.V.; Tulibaeva, G.Z.; Khatmullina, K.G.; Dorofeeva, T.V.; Yarmolenko, O.V. Empirical Formula for the Concentration Dependence of the Conductivity of Organic Electrolytes for Lithium Power Sources in the Vicinity of a Maximum. *Russ. J. Electrochem.* **2014**, *50*, 1027–1035. [CrossRef]
18. Linden, D.; Reddy, T.B. (Eds.) Handbook of Batteries. In *McGraw-Hill Handbooks*, 3rd ed.; McGraw-Hill: New York, NY, USA, 2002; ISBN 978-0-07-135978-8.
19. Younesi, R.; Veith, G.M.; Johansson, P.; Edström, K.; Vegge, T. Lithium Salts for Advanced Lithium Batteries: Li–Metal, Li–O_2, and Li–S. *Energy Environ. Sci.* **2015**, *8*, 1905–1922. [CrossRef]
20. Marcinek, M.; Syzdek, J.; Marczewski, M.; Piszcz, M.; Niedzicki, L.; Kalita, M.; Plewa-Marczewska, A.; Bitner, A.; Wieczorek, P.; Trzeciak, T.; et al. Electrolytes for Li-Ion Transport–Review. *Solid State Ionics* **2015**, *276*, 107–126. [CrossRef]
21. Deng, J.; Bae, C.; Marcicki, J.; Masias, A.; Miller, T. Safety Modelling and Testing of Lithium-Ion Batteries in Electrified Vehicles. *Nat. Energy* **2018**, *3*, 261–266. [CrossRef]
22. Jiang, L.; Wang, Q.; Li, K.; Ping, P.; Jiang, L.; Sun, J. A Self-Cooling and Flame-Retardant Electrolyte for Safer Lithium Ion Batteries. *Sustain. Energy Fuels* **2018**, *2*, 1323–1331. [CrossRef]
23. Armand, M.; Chabango, J.M.; Duclot, M. Polymeric Solid Electrolytes. In Proceedings of the 2th International Meeting on Solid Electrolytes, St Andrews, Scotland, 20–22 September 1978; p. 6.

24. Yarmolenko, O.V.; Khatmullina, K.G.; Tulibaeva, G.Z.; Bogdanova, L.M.; Shestakov, A.F. Towards the Mechanism of Li^+ Ion Transfer in the Net Solid Polymer Electrolyte Based on Polyethylene Glycol Diacrylate–$LiClO_4$. *J. Solid State Electrochem.* **2012**, *16*, 3371–3381. [CrossRef]

25. Sun, C.; Wang, Z.; Yin, L.; Xu, S.; Ghazi, Z.A.; Shi, Y.; An, B.; Sun, Z.; Cheng, H.-M.; Li, F. Fast Lithium Ion Transport in Solid Polymer Electrolytes from Polysulfide-Bridged Copolymers. *Nano Energy* **2020**, *75*, 104976. [CrossRef]

26. Li, X.; Zheng, Y.; Duan, Y.; Shang, M.; Niu, J.; Li, C.Y. Designing Comb-Chain Crosslinker-Based Solid Polymer Electrolytes for Additive-Free All-Solid-State Lithium Metal Batteries. *Nano Lett.* **2020**, *20*, 6914–6921. [CrossRef] [PubMed]

27. Paranjape, N.; Mandadapu, P.C.; Wu, G.; Lin, H. Highly-Branched Cross-Linked Poly (Ethylene Oxide) with Enhanced Ionic Conductivity. *Polymer* **2017**, *111*, 1–8. [CrossRef]

28. Ibrahim, S.; Yassin, M.M.; Ahmad, R.; Johan, M.R. Effects of Various $LiPF_6$ Salt Concentrations on PEO-Based Solid Polymer Electrolytes. *Ionics* **2011**, *17*, 399–405. [CrossRef]

29. Meabe, L.; Huynh, T.V.; Mantione, D.; Porcarelli, L.; Li, C.; O'Dell, L.A.; Sardon, H.; Armand, M.; Forsyth, M.; Mecerreyes, D. UV-Cross-Linked Poly(Ethylene Oxide Carbonate) as Free Standing Solid Polymer Electrolyte for Lithium Batteries. *Electrochim. Acta* **2019**, *302*, 414–421. [CrossRef]

30. Shim, J.; Kim, L.; Kim, H.J.; Jeong, D.; Lee, J.H.; Lee, J.-C. All-Solid-State Lithium Metal Battery with Solid Polymer Electrolytes Based on PolysiloxaneCrosslinked by Modified Natural Gallic Acid. *Polymer* **2017**, *122*, 222–231. [CrossRef]

31. LaCoste, J.; Li, Z.; Xu, Y.; He, Z.; Matherne, D.; Zakutayev, A.; Fei, L. Investigating the Effects of Lithium Phosphorous Oxynitride Coating on Blended Solid Polymer Electrolytes. *ACS Appl. Mater. Interfaces* **2020**, *12*, 40749–40758. [CrossRef]

32. Mackanic, D.G.; Michaels, W.; Lee, M.; Feng, D.; Lopez, J.; Qin, J.; Cui, Y.; Bao, Z. Crosslinked Poly(Tetrahydrofuran) as a Loosely Coordinating Polymer Electrolyte. *Adv. Energy Mater.* **2018**, *8*, 1800703. [CrossRef]

33. Timachova, K.; Villaluenga, I.; Cirrincione, L.; Gobet, M.; Bhattacharya, R.; Jiang, X.; Newman, J.; Madsen, L.A.; Greenbaum, S.G.; Balsara, N.P. Anisotropic Ion Diffusion and Electrochemically Driven Transport in Nanostructured Block Copolymer Electrolytes. *J. Phys. Chem. B* **2018**, *122*, 1537–1544. [CrossRef] [PubMed]

34. Fu, X.; Liu, Y.; Wang, W.; Han, L.; Yang, J.; Ge, M.; Yao, Y.; Liu, H. Probing the Fast Lithium-Ion Transport in Small-Molecule Solid Polymer Electrolytes by Solid-State NMR. *Macromolecules* **2020**, *53*, 10078–10085. [CrossRef]

35. Sangeetha, M.; Mallikarjun, A.; Reddy, M.J.; Kumar, J.S. FTIR Spectroscopic and DC Ionic Conductivity Studies of PVDF-HFP: $LiBF_4$: EC Plasticized Polymer Electrolyte Membrane. *IOP Conf. Ser. Mater. Sci. Eng.* **2017**, *225*, 12049. [CrossRef]

36. Khatmullina, K.G.; Baimuratova, G.R.; Lesnichaya, V.A.; Shuvalova, N.I.; Yarmolenko, O.V. Mechanical and Electrochemical Properties of New Nanocomposite Polymer Electrolytes Based on Poly(vinylidene fluoride) Copolymer with Hexafluoropropylene and SiO_2 Addition. *Polym. Sci. Ser. A* **2018**, *60*, 222–228. [CrossRef]

37. Jia, H.; Onishi, H.; Wagner, R.; Winter, M.; Cekic-Laskovic, I. Intrinsically Safe Gel Polymer Electrolyte Comprising Flame-Retarding Polymer Matrix for Lithium Ion Battery Application. *ACS Appl. Mater. Interfaces* **2018**, *10*, 42348–42355. [CrossRef]

38. Janakiraman, S.; Padmaraj, O.; Ghosh, S.; Venimadhav, A. A Porous Poly (Vinylidene Fluoride-Co-Hexafluoropropylene) Based Separator-Cum-Gel Polymer Electrolyte for Sodium-Ion Battery. *J. Electroanal. Chem.* **2018**, *826*, 142–149. [CrossRef]

39. Krause, C.H.; Röring, P.; Onishi, H.; Diddens, D.; Thienenkamp, J.H.; Brunklaus, G.; Winter, M.; Cekic-Laskovic, I. Propylene Carbonate-Nitrile Solvent Blends for Thermally Stable Gel Polymer Lithium Ion Battery Electrolytes. *J. Power Sources* **2020**, *478*, 229047. [CrossRef]

40. Poiana, R.; Lufrano, E.; Tsurumaki, A.; Simari, C.; Nicotera, I.; Navarra, M.A. Safe Gel Polymer Electrolytes for High Voltage Li-Batteries. *Electrochim. Acta* **2022**, *401*, 139470. [CrossRef]

41. Zhu, Y.; Wang, F.; Liu, L.; Xiao, S.; Chang, Z.; Wu, Y. Composite of a nonwoven fabric with poly (vinylidene fluoride) as a gel membrane of high safety for lithium ion battery. *Energy Environ. Sci.* **2013**, *6*, 618–624. [CrossRef]

42. Richardson, P.M.; Voice, A.M.; Ward, I.M. NMR self-diffusion and relaxation time measurements for poly (vinylidene fluoride) (PVDF) based polymer gel electrolytes containing $LiBF_4$ and propylene carbonate. *Polymer* **2016**, *97*, 69–79. [CrossRef]

43. Zhang, H.; Ma, X.; Lin, C.; Zhu, B. Gel polymer electrolyte based on PVDF/fluorinated amphiphilic copolymer blends for high performance lithium-ion batteries. *RSC Adv.* **2014**, *4*, 33713–33719. [CrossRef]

44. Deng, F.; Wang, X.; He, D.; Hu, J.; Gong, C.; Ye, Y.S.; Xie, X.; Xue, Z. Microporous polymer electrolyte based on PVDF/PEO star polymer blends for lithium ion batteries. *J. Membr. Sci.* **2015**, *491*, 82–89. [CrossRef]

45. Xiao, S.Y.; Yang, Y.Q.; Li, M.X.; Wang, F.X.; Chang, Z.; Wu, Y.P.; Liu, X. A composite membrane based on a biocompatible cellulose as a hostof gel polymer electrolyte for lithium ion batteries. *J. Power Sources* **2014**, *270*, 53–58. [CrossRef]

46. Hosseinioun, A.; Nurnberg, P.; Schonho, M.; Diddens, D.; Paillard, E. Improved lithium ion dynamics in crosslinked PMMA gel polymer electrolyte. *RSC Adv.* **2019**, *9*, 27574–27582. [CrossRef]

47. Garaga, M.N.; Jayakody, N.; Fraenza, C.C.; Itin, B.; Greenbaum, S. Molecular-level insights into structure and dynamics in ionic liquids and polymer gel electrolytes. *J. Mol. Liq.* **2021**, *329*, 115454. [CrossRef]

48. Hu, P.; Zhao, J.; Wang, T.; Shang, C.; Zhang, J.; Qin, B.; Liu, Z.; Xiong, J.; Cui, G. A composite gel polymer electrolyte with high voltage cyclability for Ni-rich cathode of lithium-ion battery. *Electrochem. Commun.* **2015**, *61*, 32–35. [CrossRef]

49. Simari, C.; Lufrano, E.; Coppola, L.; Nicotera, I. Composite Gel Polymer Electrolytes Based on Organo-Modified Nanoclays: Investigation on Lithium-Ion Transport and Mechanical Properties. *Membranes* **2018**, *8*, 69. [CrossRef]

50. Rosenwinkel, M.P.; Schönhof, M. Polymer-Induced Inversion of the Li^+ Drift Direction in Ionic Liquid-Based Ternary Polymer Electrolytes. *Macromol. Chem. Phys.* **2021**, 2100320. [CrossRef]

51. Wang, B.-H.; Xia, T.; Chen, Q.; Yao, Y.-F. Probing the Dynamics of Li$^+$ Ions on the Crystal Surface: A Solid-State NMR Study. *Polymers* **2020**, *12*, 391. [CrossRef]

52. Zheng, J.; Liu, X.; Duan, Y.; Chen, L.; Zhang, X.; Feng, X.; Chen, W.; Zhao, Y. Stable cross-linked gel terpolymer electrolyte containing methyl phosphonate for sodium ion batteries. *J. Membr. Sci.* **2019**, *583*, 163–170. [CrossRef]

53. Marinin, A.A.; Khatmullina, K.G.; Volkov, V.I.; Yarmolenko, O.V. Self-Diffusion of Lithium Cations and Ionic Conductivity in Polymer Electrolytes Based on Polyesterdiacrylate. *Russ. J. Electrochem.* **2011**, *47*, 717–725. [CrossRef]

54. Marinin, A.A.; Khatmullina, K.G.; Volkov, V.I.; Yarmolenko, O.V.; Zabrodin, V.A. Structures of Polymer Electrolytes Based on Polyester Diacrylate: An NMR Study. *Russ. Chem. Bull.* **2011**, *60*, 1096–1100. [CrossRef]

55. Yarmolenko, O.V.; Khatmullina, K.G.; Kurmaz, S.V.; Baturina, A.A.; Bubnova, M.L.; Shuvalova, N.I.; Grachev, V.P.; Efimov, O.N. New lithium-conducting gel electrolytes containing superbranched polymers. *Russ. J. Electrochem.* **2013**, *49*, 252–258. [CrossRef]

56. Verdier, N.; Lepage, D.; Zidani, R.; Prébé, A.; Aymé-Perrot, D.; Pellerin, C.; Dollé, M.; Rochefort, D. Crosslinked polyacrylonitrile-based elastomer used as gel polymer electrolyte in Li-ion battery. *ACS Appl. Energy Mater.* **2020**, *3*, 1099–1110. [CrossRef]

57. Porthault, H.; Piana, G.; Duffault, J.M.; Franger, S. Influence of ionic interactions on lithium diffusion properties in ionic liquid-based gel polymer electrolytes. *Electrochim. Acta* **2020**, *354*, 136632. [CrossRef]

58. Chernyak, A.V.; Yudina, A.V.; Yarmolenko, O.V.; Volkov, V.I. NMR Study of the Polyethylene Glycol Diacrylate-LiBF$_4$-1-Butyl-3-Methylimidazolium Tetrafluoroborate-Propylene/Ethylene Carbonate Electrolyte System. *Russ. J. Electrochem.* **2015**, *51*, 478–482. [CrossRef]

59. Yarmolenko, O.V.; Yudina, A.V.; Evshchik, E.Y.; Chernyak, A.V.; Marinin, A.A.; Volkov, V.I.; Kulova, T.L. New Network-Gel-Electrolytes Consisting of Polyethylene Glycol Diacrylate, LiBF$_4$, and 1-Butyl-3-Methylimidazolium Tetrafluoroborate, Added with Alkylene Carbonates: The Ion Transfer Mechanism and Properties. *Russ. J. Electrochem.* **2015**, *51*, 421–428. [CrossRef]

60. Chernyak, A.V.; Berezin, M.P.; Slesarenko, N.A.; Zabrodin, V.A.; Volkov, V.I.; Yudina, A.V.; Shuvalova, N.I.; Yarmolenko, O.V. Influence of the Reticular Polymeric Gel-Electrolyte Structure on Ionic and Molecular Mobility of an Electrolyte System Salt-Ionic Liquid: LiBF$_4$-1-Ethyl-3-Methylimidazolium Tetrafluoroborate. *Russ. Chem. Bull.* **2016**, *65*, 2053–2058. [CrossRef]

61. Yarmolenko, O.V.; Yudina, A.V.; Ignatova, A.A.; Shuvalova, N.I.; Martynenko, V.M.; Bogdanova, L.M.; Chernyak, A.V.; Zabrodin, V.A.; Volkov, V.I. New Polymer Electrolytes Based on Polyethylene Glycol Diacrylate–LiBF$_4$–1-Ethyl-3-Methylimidazolium Tetrafluoroborate with the Introduction of Alkylene Carbonates. *Russ. Chem. Bull.* **2015**, *64*, 2505–2511. [CrossRef]

62. Yarmolenko, O.V. New Polymer Electrolytes Modified with Crown-Ethers for Lithium Power Sources. Ph.D. Thesis, The Institute of Physical Chemistry and Electrochemistry RAS (IPCE RAS), Moscow, Russia, 17 April 2012.

63. Zheng, J.; Hu, Y.-Y. New Insights into the Compositional Dependence of Li-Ion Transport in Polymer-Ceramic Composite Electrolytes. *ACS Appl. Mater. Interfaces* **2018**, *10*, 4113–4120. [CrossRef]

64. Yarmolenko, O.V.; Khatmullina, K.G.; Baimuratova, G.R.; Tulibaeva, G.Z.; Bogdanova, L.M.; Shestakov, A.F. On the Nature of the Double Maximum Conductivity of Nanocomposite Polymer Electrolytes for Lithium Power Sources. *Mendeleev Comm.* **2018**, *28*, 41–43. [CrossRef]

65. Baymuratova, G.R.; Chernyak, A.V.; Slesarenko, A.A.; Tulibaeva, G.Z.; Volkov, V.I.; Yarmolenko, O.V. Specific Features of Ion Transport in New Nanocomposite Gel Electrolytes Based on Cross-Linked Polymers and Silica Nanoparicles. *Russ. J. Electrochem.* **2019**, *55*, 529–536. [CrossRef]

66. Liu, X.; Li, X.; Li, H.; Wu, H.B. Recent Progress of Hybrid Solid-State Electrolytes for Lithium Batteries. *Chem. Eur. J.* **2018**, *24*, 18293–18306. [CrossRef] [PubMed]

67. Li, Y.; Xu, B.; Xu, H.; Duan, H.; Lü, X.; Xin, S.; Zhou, W.; Xue, L.; Fu, G.; Manthiram, A.; et al. Hybrid Polymer/Garnet Electrolyte with a Small Interfacial Resistance for Lithium-Ion Batteries. *Angew. Chem. Int. Ed.* **2017**, *56*, 753–756. [CrossRef]

68. Polu, A.R.; Rhee, H.-W. Nanocomposite solid polymer electrolytes based on poly(ethylene oxide)/POSS-PEG (n=13.3) hybrid nanoparticles for lithium ion batteries. *J. Ind. Eng. Chem.* **2015**, *31*, 323–329. [CrossRef]

69. Zhang, J.; Li, X.; Li, Y.; Wang, H.; Ma, C.; Wang, Y.; Hu, S.; Wei, W. Cross-Linked Nanohybrid Polymer Electrolytes with POSS Cross-Linker for Solid-State Lithium Ion Batteries. *Front. Chem.* **2018**, *6*, 186–196. [CrossRef] [PubMed]

70. Zhu, Y.; Xiao, S.; Shi, Y.; Yang, Y.; Hou, Y.; Wu, Y. A composite gel polymer electrolyte with high performance based on poly(vinylidene fluoride) and polyborate for lithium ion batteries. *Adv. Energy Mater.* **2014**, *4*, 1300647–1300656. [CrossRef]

71. Tan, X.; Wu, Y.; Tang, W.; Song, S.; Yao, J.; Wen, Z.; Lu, L.; Savilov, S.V.; Hu, N.; Molenda, J. Preparation of Nanocomposite Polymer Electrolyte via In Situ Synthesis of SiO$_2$ Nanoparticles in PEO. *Nanomaterials* **2020**, *10*, 157. [CrossRef]

72. Menkin, S.; Lifshitz, M.; Haimovich, A.; Goor, M.; Blanga, R.; Greenbaum, S.G.; Goldbourt, A.; Golodnitsky, D. Evaluation of ion-transport in composite polymer-in-ceramic electrolytes. Case study of active and inert ceramics. *Electrochim. Acta* **2019**, *304*, 447–455. [CrossRef]

73. Wu, N.; Chien, P.-H.; Qian, Y.; Li, Y.; Xu, H.; Grundish, N.S.; Xu, B.; Jin, H.; Hu, Y.-Y.; Yu, G.; et al. Enhanced Surface Interactions Enable Fast Li$^+$ Conduction in Oxide/Polymer Composite Electrolyte. *Angew. Chem. Int. Ed.* **2020**, *59*, 4131–4137. [CrossRef]

74. Wang, Z.; Wang, S.; Wang, A.; Liu, X.; Chen, J.; Zeng, Q.; Zhang, L.; Liu, W.; Zhang, L. Covalently linked metal–organic framework (MOF)-polymer all-solid-state electrolyte membranes for room temperature high performance lithium batteries. *J. Mater. Chem. A* **2018**, *6*, 17227–17234. [CrossRef]

75. Hu, J.; Wang, W.; Zhou, B.; Feng, Y.; Xie, X.; Xue, Z. Poly(ethylene oxide)-based composite polymer electrolytes embedding with ionic bond modified nanoparticles for all-solid-state lithium-ion battery. *J. Membr. Sci.* **2019**, *575*, 200–208. [CrossRef]

76. Yang, H.; Bright, J.; Chen, B.; Zheng, P.; Gao, X.; Liu, B.; Kasani, S.; Zhang, X.; Wu, N. Chemical interaction and enhanced interfacial ion transport in a ceramic nanofiber–polymer composite electrolyte for all-solid-state lithium metal batteries. *J. Mater. Chem. A* **2020**, *8*, 7261. [CrossRef]

77. Al-Salih, H.; Huang, A.; Yim, C.-H.; Freytag, A.I.; Goward, G.R.; Baranova, E.; Abu-Lebdeh, Y. A Polymer-Rich Quaternary Composite Solid Electrolyte for Lithium Batteries. *J. Electrochem. Soc.* **2020**, *167*, 70557. [CrossRef]

78. Banitaba, S.N.; Semnani, D.; Heydari-Soureshjani, E.; Rezaei, B.; Ensafi, A.A. Electrospun Core-shell Nanofibers Based on Polyethylene Oxide Reinforced by Multiwalled Carbon Nanotube and Silicon Dioxide Nanofillers: A Novel and Effective Solvent-free Electrolyte for Lithium Ion Batteries. *Int. J. Energy Res.* **2020**, *44*, 7000–7014. [CrossRef]

79. Klongkan, S.; Pumchusak, J. Effects of Nano Alumina and Plasticizers on Morphology, Ionic Conductivity, Thermal and Mechanical Properties of PEO-LiCF3SO3 Solid Polymer Electrolyte. *Electrochim. Acta* **2015**, *161*, 171–176. [CrossRef]

80. Carbone, L.; Gobet, M.; Peng, J.; Devany, M.; Scrosati, B.; Greenbaum, S.; Hassoun, J. Polyethylene glycol dimethyl ether (PEGDME)-based electrolyte for lithium metal battery. *J. Power Sources* **2015**, *299*, 460–464. [CrossRef]

81. Rathod, S.G.; Bhajantri, R.F.; Ravindrachary, V.; Sheela, T.; Pujari, P.K.; Naik, J.; Poojary, B. Pressure Sensitive Dielectric Properties of TiO_2 Doped PVA/CN-Li Nanocomposite. *J. Polym. Res.* **2015**, *22*, 6. [CrossRef]

82. Wu, J.; Zuo, X.; Chen, Q.; Deng, X.; Liang, H.; Zhu, T.; Liu, J.; Li, W.; Nan, J. Functional Composite Polymer Electrolytes with Imidazole Modified SiO_2 Nanoparticles for High-Voltage Cathode Lithium Ion Batteries. *Electrochim. Acta* **2019**, *320*, 134567. [CrossRef]

83. Bose, P.; Deb, D.; Bhattacharya, S. Lithium-polymer battery with ionic liquid tethered nanoparticles incorporated (PVDF-HFP) nanocomposite gel polymer electrolyte. *Electrochim. Acta* **2019**, *319*, 753–765. [CrossRef]

84. Verma, H.; Mishra, K.; Rai, D.K. Sodium ion conducting nanocomposite polymer electrolyte membrane for sodium ion batteries. *J. Solid State Electrochem.* **2020**, *24*, 521–532. [CrossRef]

85. Kumar, D.; Suleman, M.; Hashmi, S.A. Studies on Poly(Vinylidene Fluoride-Co-Hexafluoropropylene) Based Gel Electrolyte Nanocomposite for Sodium–Sulfur Batteries. *Solid State Ionics* **2011**, *202*, 45–53. [CrossRef]

86. Mishra, K.; Rai, D.K. Studies on Ionic Liquid Based Nanocomposite Gel Polymer Electrolyte and Its Application in Sodium Battery. *Mater. Sci. Eng. B* **2021**, *267*, 115098. [CrossRef]

87. Pradeepa, P.; Edwinraj, S.; Ramesh Prabhu, M. Effects of Ceramic Filler in Poly(Vinyl Chloride)/Poly(Ethyl Methacrylate) Based Polymer Blend Electrolytes. *Chin. Chem. Lett.* **2015**, *26*, 1191–1196. [CrossRef]

88. Tang, S.; Lan, Q.; Xu, L.; Liang, J.; Lou, P.; Liu, C.; Mai, L.; Cao, Y.-C.; Cheng, S. A Novel Cross-Linked Nanocomposite Solid-State Electrolyte with Super Flexibility and Performance for Lithium Metal Battery. *Nano Energy* **2020**, *71*, 104600. [CrossRef]

89. Xie, H.; Liao, Y.; Sun, P.; Chen, T.; Rao, M.; Li, W. Investigation on Polyethylene-Supported and Nano-SiO_2 Doped Poly(Methyl Methacrylate-Co-Butyl Acrylate) Based Gel Polymer Electrolyte for High Voltage Lithium Ion Battery. *Electrochim. Acta* **2014**, *127*, 327–333. [CrossRef]

90. Pal, P.; Ghosh, A. Influence of TiO_2 nano-particles on charge carrier transport and cell performance of PMMA-$LiClO_4$ based nano-composite electrolytes. *Electrochim. Acta.* **2017**, *260*, 157–167. [CrossRef]

91. Yarmolenko, O.V.; Khatmullina, K.G.; Bogdanova, L.M.; Shuvalova, N.I.; Dzhavadyan, E.A.; Marinin, A.A.; Volkov, V.I. Effect of TiO_2 Nanoparticle Additions on the Conductivity of Network Polymer Electrolytes for Lithium Power Sources. *Russ. J. Electrochem.* **2014**, *50*, 336–344. [CrossRef]

92. Yarmolenko, O.V.; Yudina, A.V.; Marinin, A.A.; Chernyak, A.V.; Volkov, V.I.; Shuvalova, N.I.; Shestakov, A.F. Nanocomposite Network Polymer Gel-Electrolytes: TiO_2- and Li_2TiO_3-Nanoparticle Effects on Their Structure and Properties. *Russ. J. Electrochem.* **2015**, *51*, 412–420. [CrossRef]

93. Lee, T.K.; Andersson, R.; Dzulkurnain, N.A.; Hernández, G.; Mindemark, J.; Brandell, D. Polyester-ZrO_2 Nanocomposite Electrolytes with High Li Transference Numbers for Ambient Temperature All-Solid-State Lithium Batteries. *Batter. Supercaps* **2021**, *4*, 653–662. [CrossRef]

94. Yudina, A.V.; Berezin, M.P.; Baymuratova, G.R.; Shuvalova, N.I.; Yarmolenko, O.V. Specific features of the synthesis and the physicochemical properties of nanocomposite polymer electrolytes based on poly(ethylene glycol) diacrylate with the introduction of SiO_2. *Russ. Chem. Bull.* **2017**, *66*, 1278–1283. [CrossRef]

95. Kumar, V.; Reddy, R.R.; Kumar, B.V.N.P.; Avadhani, C.V.; Ganapathy, S.; Chandrakumar, N.; Sivaram, S. Lithium Speciation in the $LiPF_6$/PC Electrolyte Studied by Two-Dimensional Heteronuclear Overhauser Enhancement and Pulse-Field Gradient Diffusometry NMR. *J. Phys. Chem. C* **2019**, *123*, 9661–9672. [CrossRef]

96. Messinger, R.J.; Vu Huynh, T.; Bouchet, R.; Sarou-Kanian, V.; Deschamps, M. Magic-Angle-Spinning-Induced Local Ordering in Polymer Electrolytes and Its Effects on Solid-State Diffusion and Relaxation NMR Measurements. *Magn. Reson. Chem.* **2020**, *58*, 1118–1129. [CrossRef] [PubMed]

97. Peng, J.; Xiao, Y.; Clarkson, D.A.; Greenbaum, S.G.; Zawodzinski, T.A.; Chen, X.C. A Nuclear Magnetic Resonance Study of Cation and Anion Dynamics in Polymer-Ceramic Composite Solid Electrolytes. *ACS Appl. Polym. Mater.* **2020**, *2*, 1180–1189. [CrossRef]

98. Takekawa, R.; Kawamura, J. Measurement of the Diffusion of Multiple Nuclei in Restricted Spaces by Pulsed Field Gradient NMR. *J. Magn. Reson.* **2021**, *326*, 106958. [CrossRef]

99. Stöffler, H.; Zinkevich, T.; Yavuz, M.; Hansen, A.-L.; Knapp, M.; Bednarčík, J.; Randau, S.; Richter, F.H.; Janek, J.; Ehrenberg, H.; et al. Amorphous versus Crystalline Li_3PS_4: Local Structural Changes during Synthesis and Li Ion Mobility. *J. Phys. Chem. C* **2019**, *123*, 10280–10290. [CrossRef]

100. Tambio, S.J.; Deschamps, M.; Sarou-Kanian, V.; Etiemble, A.; Douillard, T.; Maire, E.; Lestriez, B. Self-Diffusion of Electrolyte Species in Model Battery Electrodes Using Magic Angle Spinning and Pulsed Field Gradient Nuclear Magnetic Resonance. *J. Power Sources* **2017**, *362*, 315–322. [CrossRef]

101. Tominaga, Y.; Yamazaki, K. Fast Li-Ion Conduction in Poly(Ethylene Carbonate)-Based Electrolytes and Composites Filled with TiO_2 Nanoparticles. *Chem. Commun.* **2014**, *50*, 4448–4450. [CrossRef]

102. Wang, Y.; Chen, W.; Zhao, Q.; Jin, G.; Xue, Z.; Wang, Y.; Mu, T. Ionicity of Deep Eutectic Solvents by Walden Plot and Pulsed Field Gradient Nuclear Magnetic Resonance (PFG-NMR). *Phys. Chem. Chem. Phys.* **2020**, *22*, 25760–25768. [CrossRef]

103. Xiang, Y.-X.; Zheng, G.; Zhong, G.; Wang, D.; Fu, R.; Yang, Y. Toward Understanding of Ion Dynamics in Highly Conductive Lithium Ion Conductors: Some Perspectives by Solid State NMR Techniques. *Solid State Ionics* **2018**, *318*, 19–26. [CrossRef]

104. Zettl, R.; Gombotz, M.; Clarkson, D.; Greenbaum, S.G.; Ngene, P.; de Jongh, P.E.; Wilkening, H.M.R. Li-Ion Diffusion in Nanoconfined $LiBH_4$-LiI/Al_2O_3: From 2D Bulk Transport to 3D Long-Range Interfacial Dynamics. *ACS Appl. Mater. Interfaces* **2020**, *12*, 38570–38583. [CrossRef] [PubMed]

105. Sata, N.; Eberman, K.; Eberl, K.; Maier, J. Mesoscopic Fast Ion Conduction in Nanometre-Scale Planar Heterostructures. *Nature* **2000**, *408*, 946–949. [CrossRef] [PubMed]

106. Maier, J. Nanoionics: Ion Transport and Electrochemical Storage in Confined Systems. *Nat. Mater.* **2005**, *4*, 805–815. [CrossRef]

107. Daigle, J.-C.; Arnold, A.; Vijh, A.; Zaghib, K. Solid-State NMR Study of New Copolymers as Solid Polymer Electrolytes. *Magnetochemistry* **2018**, *4*, 13. [CrossRef]

108. Foran, G.; Verdier, N.; Lepage, D.; Malveau, C.; Dupré, N.; Dollé, M. Use of Solid-State NMR Spectroscopy for the Characterization of Molecular Structure and Dynamics in Solid Polymer and Hybrid Electrolytes. *Polymers* **2021**, *13*, 1207. [CrossRef] [PubMed]

109. Ranque, P.; Zagórski, J.; Devaraj, S.; Aguesse, F.; López del Amo, J.M. Characterization of the Interfacial Li-Ion Exchange Process in a Ceramic-Polymer Composite by Solid State NMR. *J. Mater. Chem. A* **2021**, *9*, 17812–17820. [CrossRef]

110. López, I.; Morey, J.; Ledeuil, J.B.; Madec, L.; Martinez, H. A Critical Discussion on the Analysis of Buried Interfaces in Li Solid-State Batteries. Ex Situ and in Situ/Operando Studies. *J. Mater. Chem. A* **2021**, *9*, 25341–25368. [CrossRef]

111. O'Donnell, L.F.; Greenbaum, S.G. Review of Multivalent Metal Ion Transport in Inorganic and Solid Polymer Electrolytes. *Batteries* **2020**, *7*, 3. [CrossRef]

112. Becher, M.; Becker, S.; Hecht, L.; Voge, M. From Local to Diffusive Dynamics in Polymer Electrolytes: NMR Studies on Coupling of Polymer and Ion Dynamics across Length and Time Scales. *Macromolecules* **2019**, *52*, 9128–9139. [CrossRef]

113. Pipertzis, A.; Papamokos, G.; Sachnik, O.; Allard, S.; Scherf, U.; Floudas, G. Ionic Conductivity in Polyfluorene-Based Diblock Copolymers Comprising Nanodomains of a Polymerized Ionic Liquid and a Solid Polymer Electrolyte Doped with LiTFSI. *Macromolecules* **2021**, *54*, 4257–4268. [CrossRef]

114. Fu, X.-B.; Yang, G.; Wu, J.-Z.; Wang, J.-C.; Chen, Q.; Yao, Y.-F. Fast Lithium-Ion Transportation in Crystalline Polymer Electrolytes. *Chem. Phys. Chem.* **2018**, *19*, 45–50. [CrossRef] [PubMed]

115. Chua, S.; Fang, R.; Sun, Z.; Wu, M.; Gu, Z.; Wang, Y.; Hart, J.N.; Sharma, N.; Li, F.; Wang, D. Hybrid Solid Polymer Electrolytes with Two-Dimensional Inorganic Nanofillers. *Chem. Eur. J.* **2018**, *24*, 18180–18203. [CrossRef]

116. Meabe, L.; Huynh, T.V.; Lago, N.; Sardon, H.; Li, C.; O'Dell, L.A.; Armand, M.; Forsyth, M.; Mecerreyes, D. Poly(Ethylene Oxide Carbonates) Solid Polymer Electrolytes for Lithium Batteries. *Electrochim. Acta* **2018**, *264*, 367–375. [CrossRef]

117. Mukbaniani, O.; Aneli, J.; Tatrishvili, T.; Markarashvili, E. Solid Polymer Electrolyte Membranes on the Basis of Fluorosiloxane Matrix. *Chemistry* **2021**, *15*, 198–204. [CrossRef]

118. Azzahari, A.D.; Selvanathan, V.; Rizwan, M.; Sonsudin, F.; Yahya, R. Conductivity or rheology? Tradeoff for competing properties in the fabrication of a gel polymer electrolyte based on chitosan-barbiturate derivative. *Ionics* **2018**, *24*, 3015–3025. [CrossRef]

119. Volkov, V.I.; Marinin, A.A. NMR Methods for Studying Ion and Molecular Transport in Polymer Electrolytes. *Russ. Chem. Rev.* **2013**, *82*, 248–272. [CrossRef]

120. Lysak, D.A.; Marinin, A.A.; Dzhimak, S.S. Investigating the Nuclear Magnetic Resonance of the Structure of Electrolyte Based on a LiClO4-Ethylene Carbonate Solution. *Bull. Russ. Acad. Sci. Phys.* **2011**, *75*, 1668–1670. [CrossRef]

121. Tulibaeva, G.Z.; Shestakov, A.F.; Volkov, V.I.; Yarmolenko, O.V. Structure of $LiBF_4$ Solvate Complexes in Ethylene Carbonate, Based on High-Resolution NMR and Quantum-Chemical Data. *Russ. J. Phys. Chem.* **2018**, *92*, 749–755. [CrossRef]

122. Saikia, D.; Chen-Yang, Y.W.; Chen, Y.T.; Li, Y.K.; Lin, S.I. 7Li NMR Spectroscopy and Ion Conduction Mechanism of Composite Gel Polymer Electrolyte: A Comparative Study with Variation of Salt and Plasticizer with Filler. *Electrochim. Acta* **2009**, *54*, 1218–1227. [CrossRef]

123. Kao, H.-M.; Chang, P.-C.; Chao, S.-W.; Lee, C.-H. 7Li NMR, Ionic Conductivity and Self-Diffusion Coefficients of Lithium Ion and Solvent of Plasticized Organic–Inorganic Hybrid Electrolyte Based on PPG-PEG-PPG Diamine and Alkoxysilanes. *Electrochim. Acta* **2006**, *52*, 1015–1027. [CrossRef]

124. Mustarelli, P.; Quartarone, E.; Capiglia, C.; Tomasi, C.; Ferloni, P.; Magistris, A. Host–Guest Interactions in Fluorinated Polymer Electrolytes: A 7Li-13C NMR Study. *J. Chem. Phys.* **1999**, *111*, 3761–3768. [CrossRef]

125. Licoccia, S.; Trombetta, M.; Capitani, D.; Proietti, N.; Romagnoli, P.; Di Vona, M.L. ATR–FTIR and NMR Spectroscopic Studies on the Structure of Polymeric Gel Electrolytes for Biomedical Applications. *Polymer* **2005**, *46*, 4670–4675. [CrossRef]

126. Volkov, V.I.; Chernyak, A.V.; Avilova, I.A.; Slesarenko, N.A.; Melnikova, D.L.; Skirda, V.D. Molecular and Ionic Diffusion in Ion Exchange Membranes and Biological Systems (Cells and Proteins) Studied by NMR. *Membranes* **2021**, *11*, 385. [CrossRef]

127. Yarmolenko, O.V.; Khatmullina, K.G.; Tulibaeva, G.Z.; Bogdanova, L.M.; Shestakov, A.F. Polymer Electrolytes Based on Poly(Ester Diacrylate), Ethylene Carbonate, and LiClO$_4$: A Relationship of the Conductivity and Structure of the Polymer According to IR Spectroscopy and Quantum Chemical Modeling Data. *Russ. Chem. Bull.* **2012**, *61*, 539–548. [CrossRef]

128. Tulibaeva, G.Z.; Chernyak, A.V.; Shestakov, A.F.; Volkov, V.I.; Yarmolenko, O.V. Solvation Environment of Lithium Ion in a LiBF$_4$–Propylene Carbonate System in the Presence of 1-Ethyl-3-Methylimidazolium Tetrafluoroborate Ionic Liquid Studied by NMR and Quantum Chemical Modeling. *Russ. Chem. Bull.* **2016**, *65*, 1727–1733. [CrossRef]

129. Nkosi, F.P.; Valvo, M.; Mindemark, J.; Dzulkurnain, N.A.; Hernández, G.; Mahun, A.; Abbrent, S.; Brus, J.; Kobera, L.; Edström, K. Garnet-Poly(ε-Caprolactone-*Co*-Trimethylene Carbonate) Polymer-in-Ceramic Composite Electrolyte for All-Solid-State Lithium-Ion Batteries. *ACS Appl. Energy Mater.* **2021**, *4*, 2531–2542. [CrossRef]

130. Popovic, J.; Brandell, D.; Ohno, S.; Hatzell, K.B.; Zheng, J.; Hu, Y.-Y. Polymer-Based Hybrid Battery Electrolytes: Theoretical Insights, Recent Advances and Challenges. *J. Mater. Chem. A* **2021**, *9*, 6050–6069. [CrossRef]

131. Mabuchi, T.; Nakajima, K.; Tokumasu, T. Molecular Dynamics Study of Ion Transport in Polymer Electrolytes of All-Solid-State Li-Ion Batteries. *Micromachines* **2021**, *12*, 1012. [CrossRef]

132. Bedrov, D.; Piquemal, J.-P.; Borodin, O.; MacKerell, A.D.; Benoît, R.; Schröder, C. Molecular Dynamics Simulations of Ionic Liquids and Electrolytes Using Polarizable Force Fields. *Chem. Rev.* **2019**, *119*, 7940–7995. [CrossRef]

133. Nilsson, V.; Bernin, D.; Brandell, D.; Edström, K.; Johansson, P. Interactions and Transport in Highly Concentrated LiTFSI-based Electrolytes. *Chem. Phys. Chem.* **2020**, *21*, 1166–1176. [CrossRef]

134. Morales, D.; Ruther, R.E.; Nanda, J.; Greenbaum, S. Ion Transport and Association Study of Glyme-Based Electrolytes with Lithium and Sodium Salts. *Electrochim. Acta* **2019**, *304*, 239–245. [CrossRef]

135. Carbone, L.; Munoz, S.; Gobet, M.; Devany, M.; Greenbaum, S.; Hassoun, J. Characteristics of Glyme Electrolytes for Sodium Battery: Nuclear Magnetic Resonance and Electrochemical Study. *Electrochim. Acta* **2017**, *231*, 223–229. [CrossRef]

136. Konefał, R.; Morávková, Z.; Paruzel, B.; Patsula, V.; Abbrent, S.; Szutkowski, K.; Jurga, S. Effect of PAMAM Dendrimers on Interactions and Transport of LiTFSI and NaTFSI in Propylene Carbonate-Based Electrolytes. *Polymers* **2020**, *12*, 1595. [CrossRef] [PubMed]